Circularly Polarised Luminescence Spectroscopy of Functionalised Lanthanide Complex for Sensing and Imaging

Osibanjo , Eniola

Durham University

MSc Thesis

CIRCULARLY POLARISED LUMINESCENCE SPECTROSCOPY OF FUNCTIONALISED LANTHANIDE COMPLEX FOR SENSING AND IMAGING

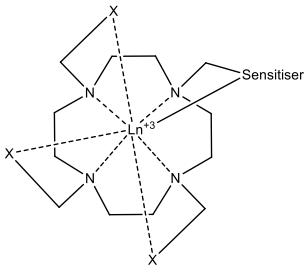

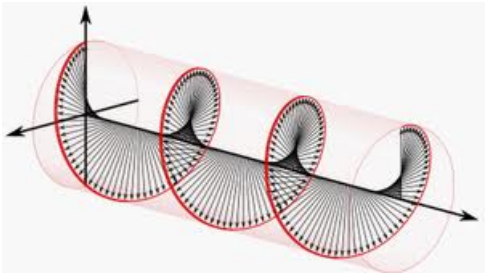

Author: **Eniola OSIBANJO**

Supervisor: **Dr Lars-Olof PÅLSSON**

Abbreviations

3-Dimensional	3D
Alternating Current	AC
Avalanche Photodiode	APD
Blue Fluorescent Protein	BFP
Cadmium	Cd
Cerium	Ce
Circular Dichroism	CD
Circular Polarisation	CP
Circularly Polarised Light	CPL
Confocal Laser Scanning Microscopy	CLSM
Direct Current	DC
Dysprosium (III)	Dy^{3+}
Electric Dipole	ED
Electroluminescence	EL
Electronic Energy Transfer	EET
Europium (III)	Eu^{3+}
Fluorescent Proteins	FPs
Gadolinium (III)	Gd^{3+}
Green Fluorescent Protein	GFP
Internal Conversion	IC
Intersystem Crossing	ISC
Iriidium	Ir
Lanthanide (III) Ions	Ln^{3+}
Lanthanum	La
Lutetium	Lu
Lock in Amplifier	LIA
Magnetic Dipole	MD
Magnetic Resonance Imaging	MRI
Monochromator	MC
Neodymium Yttrium Aluminium Garnet	Nd: YAG
Nuclear Instrumentation Module	NIM
Organic Light Emitting Diode	OLED

Osmium	Os
Photo-elastic Modulator	PEM
Photo Luminescence Quantum Yield	PLQY
Photo Luminescence	PL
Photomultiplier Tube	PMT
Platinum	Pt
Quantum Dots	QDs
Ruthenium	Ru
Samarium (III)	Sm^{3+}
Selenium	Se
Terbium	Tb
Transistor-Transistor Logic	TTL
Ultra Violet	UV
Yellow Fluorescent Protein	YFP

Abstract

This work is based on circularly polarised luminescence spectroscopy of functionalised Lanthanide (III) ion complexes that can be used for sensing and imaging. Work was also done to design optical acquisition systems for the accessories to a confocal microscope that would be modified to facilitate measurements of circularly polarised luminescence for bio-imaging. This work describes some aspects of the interactions between chiral biological molecules and functionalised optical emissive probes. The interaction between a target analyte (the biological molecule) and the probe results in a modulation of the polarisation of the emission, which is readily, studied using circularly polarised luminescence spectroscopy. Circularly polarised luminescence spectroscopy is based on the differential emission of left and right circularly polarized radiation by luminescent chiral systems. The primary observables in circularly polarised luminescence spectroscopy are the emission circular intensity differential. The systems used in this study are the luminescent Lanthanide (III) ion complexes, which have proven to be a productive area of research due to their unique optical properties enabling their use in a wide range of applications. A major drawback to using Lanthanide (III) ion is their low extinction coefficients; hence the antenna effect is often used to overcome this problem. In this way, the antenna chromophore absorbs incoming radiation and transfers the energy to the Lanthanide leading to indirect excitation of the Lanthanide (III) ion. These and similar complexes have shown an ability to bind to biologically important anions such as carbonate and phosphate in aqueous media and are able to report this event by a modulation in the Photo luminescence. These interactions have also been investigated by monitoring the emitted circularly polarised light using the technique described. Typical circularly polarised luminescence spectra of the europium (III) ion complexes will be presented as will the binding study results and a detailed account of how the spectra is obtained.

Table of Contents:

1 INTRODUCTION.

1.1 Aim.

The aim of this work was to characterise some functionalised Ln^{3+} complexes with respect to their structure and function relationship using CPL spectroscopy. These complexes are chiral structures and as such they emit CPL. The aim was to investigate the relationship between the Ln^{3+} complex and the polarisation direction of the CPL.

The secondary aim of the project was to develop a technique for analysis of Ln^{3+} complexes using CPL microscopy to be used for bio-imaging. The precursor to CPL microscopy is CPL spectroscopy. These methodologies are related techniques based on the use functionalised chiral Ln^{3+} complexes. Further experiments and investigations were therefore also performed for the analysis of Ln^{3+} complexes in the presence of specific anions using CPL spectroscopy with the aim to understand the modulation of the CPL by stereo-specific interactions.

1.2 Introduction to Lanthanides and Their Applications.

Lanthanides were first discovered in Sweden by Carl Axel Arrhenius, a Swedish Chemist in a small town called Ytterby near Stockholm, where he found a very dense black mineral known as Gadolinite[1], although at the time, there were speculations that the mineral in question might contain the element tungsten. The mineral was later investigated in 1794 by another Swedish Chemist, Johann Gadolin, who discovered that it contained oxides of iron, beryllium, silicon and a new previously unidentified element, which he named yttria. Yttria was later shown to be a mixture of the oxides of six different lanthanides. Now often referred to as rare earth elements, lanthanides consist of fifteen metallic elements ranging from La to Lu located in block $4f$ of the periodic table.

Lanthanides have many uses in science and engineering. In their various applications, lanthanides can exist in many forms including aqueous ions, complexes, alloys and pure metals. Ln^{3+} complexes can also be dissolved in mainly polar solvents such as ethanol or methanol and most importantly in water.

For PL applications, the Ln^{3+} complexes possess a very stable and prevalent oxidation state of +3 in aqueous solution and have a ground state configuration of

[Xe] $4f^n$ $5d^1$ $6s^2$, where n ranges from zero (La^{3+}) to fourteen (Lu^{3+}). With the Ln^{3+} ion characterised by their incompletely filled $4f$ shell, the $4f$ orbitals lie close to the nucleus and are well shielded from the surroundings by the outer filled $5s^2$ and $5p^6$ orbitals. The stable +3 state of the Ln^{3+} ion is obtained by the removal of the two electrons in the 6s orbital and one from the 5d or 4f orbital. However, there is an exception with Ce^{4+} and Eu^{2+} where the ion can attain an empty (f^0), half filled (f^7), or filled (f^{14}) subshell. Cerium exhibits an oxidation state of +4 since it can obtain an empty 4f orbital by the loss of four electrons and Eu^{2+} prefers oxidation state of +2. The $4f - 4f$ transitions are parity-forbidden and have very low molar absorption coefficients typically (<3 M^{-1} cm^{-1}) [2]. As a result, they are not available for bonding and the influence of the chemical environment, especially the effect of the ligands on the $4f^n$, configuration is insignificant. The coordination number, which ranges from 6-12, decreases across the series due to the lanthanide contraction.[3] This is due to the $4f$ electrons, which are rather ineffective at screening the nucleus from the peripheral electrons, hence as the nuclear charge increases, there is a subsequent contraction in ionic radius.[4]

There are today numerous applications of emissive Ln^{3+} ions in solid or in liquid state. Light devices such as fluorescent lamps and OLEDs, television and computer displays, optical fibres, optical amplifiers, lasers, as well as responsive luminescent stains for biomedical analysis, medical diagnosis, and cell imaging rely heavily on Ln^{3+} ions. Examples include the use of Eu^{3+} doped yttrium vanadate in the area of display applications as the first red phosphor to enable the development of colour television screens.[5] In optical engineering Ln^{3+} ions are used as dopants in crystalline hosts which are subsequently used as gain medium in amplifiers and laser systems, the widely used Nd:YAG laser system is the most prominent example in this context. [6]

Other applications of Ln^{3+} complexes in the life-sciences includes the use of Gadolinium Gd^{3+} complexes in MRI as contrast reagents.[7]

One of the most recent uses of Ln^{3+} ions which is related to this project is their use as biological imaging agents and PL probes in live cell imaging. Their usefulness in this application is due to their unique PL properties. Ln^{3+} complexes possess unusual optical properties that make them different, and in some cases better alternatives when compared to other typical fluorescence based systems. These

properties include millisecond lifetimes due to the symmetry forbidden (Laporte) [8] nature of the electronic transitions in the 4f manifold, characteristic narrow-line emission with a broad range of emission energies extending from the blue to the red part of the emission spectrum, high PLQYs and large Stokes shifts combined with detailed information about the factors that influence the PL. [9]

1.3 Ln^{3+} Complexes and Photo Luminescence.

As mentioned previously, Ln^{3+} complexes exhibit narrow emission lines at well-defined wavelengths with characteristic emission for each Ln^{3+} ion. The PL emission lines can be located in the ultraviolet (Gd^{3+}), visible (Eu^{3+} ranges from 570-720 nm and Tb^{3+} from 450-650 nm) or near-infrared (neodymium, ytterbium and erbium) part of the electromagnetic spectrum. Each Ln^{3+} ion has its specific emission colour. For example Eu^{3+} emits red light and Tb^{3+} emits green light.

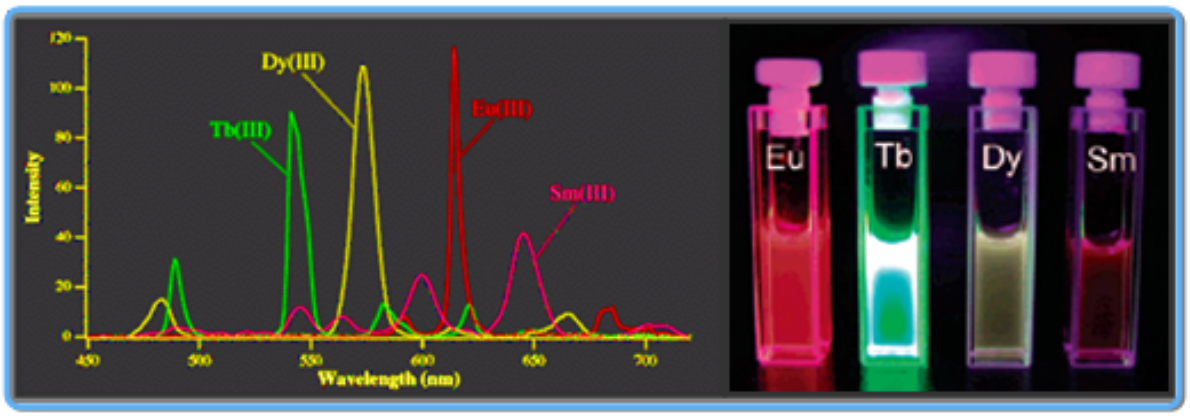

Figure 1.1 Visible emitting lanthanides Eu^{3+}, Tb^{3+}, Dy^{3+} and Sm^{3+}, each with a characteristic PL colour.[10]

As the electronic transitions of Ln^{3+} are forbidden by symmetry, it is extremely difficult to directly excite the Ln^{3+} ion through an optical excitation. To overcome this, a typical Ln^{3+} complex is functionalised with a ligand and a sensitizer (organic chromophore) designed to harvest incident light efficiently and facilitate intramolecular EET to the emissive Ln^{3+} ion.[11]

1.4 Functionalised Ln^{3+} Complexation.

Due to the unusual optical properties they possess, emissive complexes of the Ln^{3+} ions are emerging as an important class of optical probes for *in vitro* use or for study of the cellular environment. [11] As important information may be encoded in the observed signal via modulation of spectral form, lifetime or circular polarisation of these complexes, their structure and function as optical probes is highly important. Ln^{3+} ions are spherical in shape. Their coordination number varies from eight to nine. Their low polarisability and high charge density accounts for their 'hard acid' like behaviour. As a result of this Ln^{3+} ions preferably bind to hard bases such as nitrogen and oxygen. Figure 1.2 shows a generic emissive Ln^{3+} complex with the Ln^{3+} ion in the coordination environment. .

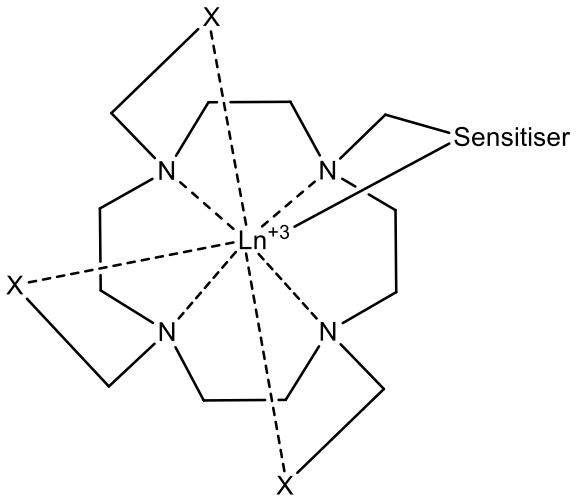

Figure 1.2: Generic structure of a functionalised Ln^{3+} (Eu^{3+}, Tb^{3+}) complex showing eight coordination including the sensitiser. X= pendant arm. Sensitiser = heterocyclic sensitising moiety.

Another key aspect in the successful use of functionalised Ln^{3+} complexes is the detailed knowledge of the factors that influence the PL output. In biological spectroscopy, this can be exploited to provide information about biological parameters as well as to monitor the physiological environments providing information on parameters such as pH, pM and pX.[11] The impact of these parameters can influence the relative intensity of emission bands, the shape of the peak (leading to ratiometric detection), the PLQY and the lifetime of the emission.

Functionalised emissive Ln^{3+} complexes are therefore excellent sensors of the chemical and biological environment. One important factor in this context is the ability to design functionalised Ln^{3+} complexes that are compatible with the biological environment.

Furthermore, functionalised Ln^{3+} complexes can be designed to be chiral systems and therefore have the ability to emit CPL. The degree of polarisation of the emission can be unusually high for these systems. The design and functional properties of the Ln^{3+} complex are important as stereochemical interactions with chiral species results in a modulation of the polarisation of the CPL. As stereo chemical interactions are highly selective, this provides a unique opportunity to study biological macromolecules and their intermolecular interactions.

1.5 Ligands for Lanthanide Complexation.

The structure of the ligand that binds to the Ln^{3+} ion is of key importance when determining the overall stability of the complex.[12] If the complex is to be used in a biological medium, then there are significant concentrations of potentially competitive chelating ligands to consider such as protein and endogenous anions. When considering the potential applications of such complexes, for example, as luminescent probes, it is critically important that the ligand should complex the appropriate lanthanide ion tightly to yield a kinetically stable and thermodynamically inert complex. The type of ligand that binds to the Ln^{3+} ion is of great importance when determining the overall stability of the Ln^{3+} complex. As the PL output of the Ln^{3+} ion can be reduced via vibronic coupling to solvent molecules, it is crucial that the ligands used are designed as cages to wrap the Ln^{3+} ion protecting it from solvent molecules. Also, it is very crucial that the ligand should complex the Ln^{3+} ion tightly to yield a kinetically stable and thermodynamically inert complex as there can be significant concentrations of chelating ligands in protein of biological medium competing with the ligand. The geometrical arrangements of the ligands are mainly controlled by steric factors and electronic repulsion between charges on the ligands. The ligand of interest should have at least eight or nine donor atoms to obtain a solvent, free complex. Some examples of ligands used are described in the pages below.

1.5.1 β-Diketone Chelates.

Ln^{3+} β-diketonate complexes were the first reported luminescent Ln^{3+} complexes and are most widely studied group of Ln^{3+} complexes today.[13] However, they are readily hydrolysed in aqueous solutions, which make them unsuitable for some applications. The substituents at the skeleton of β-diketonate ligands can vary from simple methyl groups to triflouromethyl groups, (substituted) phenyl groups, or polyaromatic moieties. The complexes can be formed as negatively charged lanthanide-tetra(β-diketonate) complexes or as neutral lanthanide-tris(β-diketonate) complexes depending on the preparation procedure. The stability of the complexes in organic solvents depends on the amount of steric hindrance between the substituents, and on the pKa of the β-diketonate ligand. The corresponding Ln^{3+} complexes are less stable with increasing acidity of the β-diketonate ligand. The main feature observed in the spectra of the Eu-tris(β-diketonate) complexes as shown by Lisa Bushby [13] is the extreme domination of the hypersensitive $\Delta J = 2$ transition resulting from the asymmetric environment of the Eu^{3+} ion.

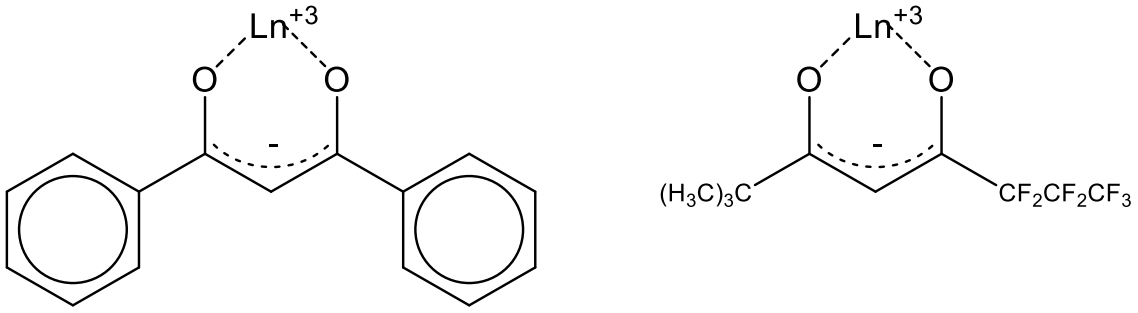

Figure 1.3 Examples of some Ln^{3+} β-diketonate complexes

1.5.2 Macrocycles/Cyclen Derivatives.

The macrocycles are another significant group of Ln^{3+} complexes. They are a large family of water soluble ligands based on the 1,4,7,10-tetraazacyclododecane skeleton (cyclen) as the core ligand element. Functionalised with donor groups such as carboxylate (DOTA), phosphinate, amide or amino acid 'arms' (e.g. DOTAM) to

the N of the cyclen ring to make up a hexa or hepta dentate moiety to shield the ion very effectively, these ligands form a cage like ligand and display extremely stable kinetic and thermodynamic properties. [14] The macrocycles also play an important role in the applications of Ln^{3+} complexes in aqueous solutions, such as MRI contrast reagents (Gd^{3+} complex) and as luminescent probes in fluoro-immuno assays (Eu^{3+} and Tb^{3+} complexes). [15] Upon pendant arm ligation, enhanced shielding from intermolecular ligation of chelating species, or quenching effects of the solvent water molecules may be achieved, resulting in increased metal-based luminescence. Depending on the charge of the donor groups, the resulting complexes may be cationic, neutral, or anionic. The complex also allows the incorporation of an antenna enabling intramolecular energy transfer for sensitisation. The macrocyclic Ln^{3+} complex can possess a number of different isomeric configurations, which depends on the nature of the Ln^{3+} ion, solvent, temperature, pressure and most importantly the nature of the ligand itself. Ln^{3+} complexes of DOTA can adopt two macrocyclic conformations labelled λλλλ and δδδδ depending on whether the NCCN chelate ring torsion angle is positive (δ) or negative (λ). There are also two possible arrangements for the side arms, (Δ) arranged in a clockwise manner and (Λ) anticlockwise manner about the metal center (with positive and negative NCCO torsion angles, respectively).[16] This leads to a formation of four possible stereoisomers, that exist as two pairs of enantiomers. (Scheme 1) However, insertion of chiral centres in the side arms inhibits arm rotation, and prevents the complex from readily interconverting between the two ring configurations.

The stereoisomers, Δ (λλλλ) and Λ (δδδδ), adopt either a monocapped square antiprismatic [17] (SAP) geometry, with a twist angle of ~40^{o} or a twisted square antiprismatic (TSAP) or trigonal prismatic intermediate geometry, with a twist angle of ~29^{o} (Δ (λλλλ) and (Λ (δδδδ)). The enantiometric pairs may interconvert between these two geometries in solution via independent cooperative pendant arm rotation (Λ ↔ Δ) or ring inversion processes (λλλλ ↔ δδδδ), typically at a rate of 50 Hz at 298K. The introduction of a substituent α or β to one of the ring nitrogen imparts conformational rigidity. Arm rotation is sterically inhibited, and ring inversion may slow down, so that one isomer in conformation may be preferentially populated in solution.

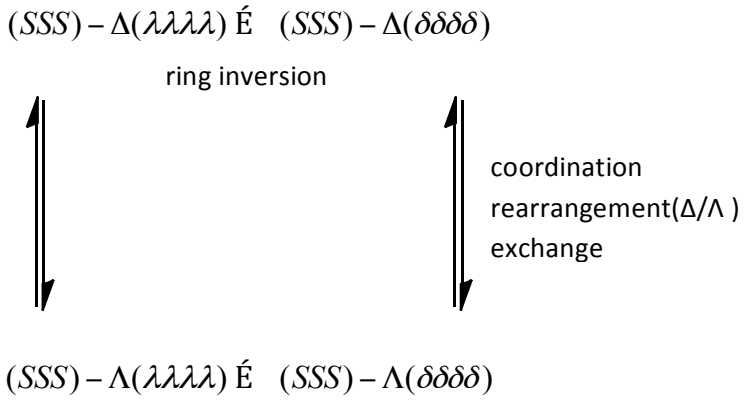

Scheme 1. The possible conversions between the different enantiomeric forms of λλλλ and δδδδ.

1.5.3 Other Ln^{3+} complexes

Examples of other Ln^{3+} complexes include EDTA[18] DTPA[19], calixarenes [20] and bipyridyl-functionalised complexes, however, these will not be further considered in this work.

1.6 Sensitiser Moiety for Lanthanide Complexation.

As described previously, the incorporation of a sensitizer to the Ln^{3+} complex is crucial for effective PL of the Ln^{3+} ion and therefore an integral part of the emissive Ln^{3+} complex. The sensitiser is a carefully selected aromatic or heterocyclic moiety; examples include acridones, azaxanthones and tetraazatriphenylenes. Mono- or bidentate coordination to the Ln^{3+} ion minimises the distance between the sensitiser and the Ln^{3+} ion, enhancing the rate of intramolecular energy transfer. The role of the sensitiser is to function as an antenna by efficiently transferring its excitation energy to the Ln^{3+} ion through a non-radiative EET process. The pendant arm shields and binds the metal ion. These functionalised Ln^{3+} complexes are therefore distinct from many of the other traditional optical probes such as organic fluorophores and QDs, which are self-contained optical chromophores. This class of materials are widely used systems today in bio-imaging.[21]

The organic chromophore needs to possess certain properties in other to be efficient as sensitiser. The properties required are; a triplet state energy of about 22,500 cm^{-1} [22] in which energy transfer can occur efficiently to the Ln^{3+} excited state, a high molar extinction coefficient such that the S_1 state is readily populated, a small singlet – triplet energy separation, minimizing ligand fluorescence and allowing

efficient inter-system crossing to populate the triplet state of the sensitiser. The main condition of triplet state is that it is 1500 cm^{-1} above the receiving energy level of the Ln^{3+} ion. If it is any higher, then efficiency of energy transfer is compromised and if it is any lower, then thermally activated back energy transfer from the Ln^{3+} exited state to the ligand becomes probable. Other important features include the ability to coordinate to the Ln^{3+} ion to minimize the sensitiser to Ln^{3+} distance. This is not only beneficial for the desired antenna-Ln^{3+} intramolecular energy transfer, but effectively shields the metal ion from intermolecular binding by maximising its coordination requirements. Furthermore, this interaction tends to inhibit the possibility of quenching by electron-transfer. Figures 1.4 and 1.5 show a few examples of organic chromophores commonly used today and their photophysical properties outlined below as revealed through a series of PL Eu^{3+} and Tb^{3+} complexes.

Tetrazatriphenylene (dpqC)

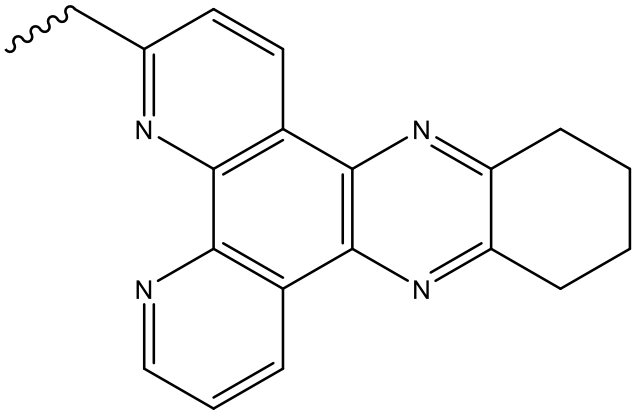

Figure 1.4 Tetrazatriphenylene. All the data are referring to measurements in H_2O.

- λmax= 348 nm, ε = 6,440 $dm^3mol^{-1}cm^{-1}$
- ET= 24,000 cm^{-1}
- Bidentate binding, q = 0
- Φ_{Eu} = 0.16, τ_{Eu} = 0.99 ms
- Φ_{Tb} = 0.40, τ_{Tb} = 1.46 ms

⇒ High quantum yields in water, with zero ligand fluorescence, although the excitation wavelength is slightly less than the >355 nm target.

Azaxanthone

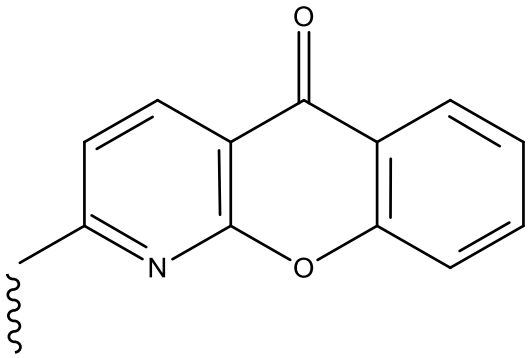

Figure 1.5 Azaxanthone. All the data are referring to measurements in H_2O.

- λmax= 336 nm, ε = 8,790 $dm^3mol^{-1}cm^{-1}$
- ET= 26,100 cm^{-1} (minimised back energy transfer)
- Φ_{Eu} = 0.07, τ_{Eu} = 0.57 ms
- Φ_{Tb} = 0.14, τ_{Tb} = 1.82 ms
- Monodentate binding, q = 1

⇒ Efficient for sensitising, with modest ligand fluorescence, but still a low excitation wavelength (can be improved by additional electron rich groups on the aromatic ring)

1.7 Introduction to Biological Spectroscopy and Bio-Imaging of Biological Systems.

Inter-molecular interactions between optical probes and biological structures or biologically relevant molecules will modulate the PL of the probe. This forms the basis for sensing in biological systems and assays. Specifically these interactions can lead to a modulation of the PLQY, which in turn can lead to both enhancement and reduction of the PLQY. The former can be due to restriction in non-radiative decay rates via hindrance of structural relaxation processes. The latter, could be caused by EET or electron transfer processes. Both these processes will also result in a modulation of the PL lifetime, which can serve as signal tool to monitor inter-molecular interactions.

Another very important and promising approach is to monitor the polarisation of the PL. In particular, the circular polarisation of the PL from a chiral emissive

complex as this PL is sensitive to the conformation or structure of the complex as previously described.

Both these methodologies have the advantage that these can be/are concentration independent methods. The PLQY is clearly a parameter that is difficult to assess in a bio-active systems as a living cell as firstly, one cannot accurately assess the probe concentration in the cell and secondly, the sample material is naturally inhomogeneous which will have adverse impact on the PL.

The ability to visualise bio-active cells is essential for a better understanding of their structure and function. Hence, imaging of biological systems is intensely pursued in life sciences to answer many fundamental questions related to cellular processes and pursued in medicine to acquire a better understanding of many of the common diseases, as these have a strong impact on cellular function.[23] Imaging is also pursued for other types of biological systems and structures such as vesicles and micelles and other forms of phase-separated architectures. Many of these systems can be entirely synthetic model systems, developed for example drug delivery.

Owing to the multiple size scales of these biological systems, it is necessary to use microscopy methodologies. A range of different imaging technologies have been pursued to date and the common challenge facing some of these techniques is usually related to the need for improved resolution. In the case where high resolution is desirable, a compromise is necessary. For example, electron microscopy can offer a resolution better than ~0.05 nm for imaging of biological structures. However, the technique is not always feasible as it requires treatment to the bio-active cell which can lead to the cell no longer being in a physiologically relevant condition.

In contrast, with the advances in molecular imaging techniques based on fluorescence techniques such as CLSM, 3D imaging, and two photon excitation fluorescence microscopy, imaging of cellular events is possible in real time in live cells. Hence, fluorescence microscopy has proven to be a very useful technique over the last few years. Fluorescence microscopy uses many different classes of PL optical probe that are selected to visualize many structural and functional properties of cells. The optical probes are mainly used as cellular stains, which are localised to particular organelles or in sub-cellular divisions. These systems include FPs, QD,

purely synthetic organic chromophores, organo-transition metal complexes and organometallic complexes.

The use of FPs in bio-imaging involves the encoding of a FP vector into cellular DNA. FP's are named after the colour of the emitted fluorescence, eg. YFP, GFP and BFP. They emit in the visible region and their excitation wavelength is above 350 nm, which makes them ideal for use in bio-imaging applications. The primary limitations of FP's in bio imaging applications include time-consuming labelling processes, complicated photo physical properties and their high molecular weight, which may perturb the structure and integrity of the bio-active cell.

QDs are often referred to as semiconductor nano-crystals with typical diameters of 2-8 nm. They constitute bright and photo-stable fluorescence sources whose emission and absorption properties can be adequately tailored through their unique size. They possess high molar extinction coefficients and high PLQYs. They also possess narrow absorption and emission bands with large Stokes shifts. They can be functionalised with anti-bodies and thus co-localise to specific cell organelles. The limitations to the use of QDs is in the means of their intracellular delivery, as labelling often requires microinjection or induced endocytosis due to their non-polar coating. [24] QDs sometimes require multiphoton excitation due to their less favourable excitation wavelength. Also, unlike Ln^{3+} complexes, QDs do not have the ability to sense the local environment; hence, they are mainly used as fluorescent tags, which can be a limitation in bio-imaging applications. There are also some concerns about the toxicity of QDs because most of these systems contain Cd or Se.[25]

In the past decade, organo-transition metal compounds showing efficient phosphorescence at ambient temperature have attracted much attention, driven especially by their applicability as phosphorescence triplet emitters in OLEDs.[26] Such complexes are constructed by chelating the transition metal ions with organic ligands and can use both the singlet and triplet excitons when incorporated into OLEDs. This can achieve maximum internal quantum efficiency of 100%. [27] They have been found to be successful for this purpose owing to their high spin–orbit coupling constants, which promote triplet radiative decay. The high spin-orbit coupling associated with the heavy metal atom can promote the triplet of singlet radiative transition, so that such complexes may exhibit unusually high phosphorescence quantum yields at room temperature and relatively short triplet emission decay times. [28] In addition, ISC

from the singlet to the triplet state (typically T_1) is also accelerated and normally depopulates the former at a rate (10^{12} s^{-1}) much faster than that of radiative emission from the singlet state (10^8-10^9 s^{-1}). [29] As a result, fluorescence is not commonly observed from discrete complexes of the third row transition-metal complexes, although a few examples are known, for example, where a ligand incorporates a π-conjugated chromophoric ligand somewhat remote from the metal center. Ir(III), Pt(II), Os(II) and Ru(II) ions are highly effective for this purpose and these complexes have the highest potential for EL applications due to their higher triplet quantum yield (ΦP), relatively short triplet state lifetime (τP), and tunable emission colour.[29]

Organic chromophores are perhaps the most widely used class of optical probes. They are highly emissive with PLQYs that are often > 0.7. They possess large molar absorption coefficients (~200 000 M^{-1} cm^{-1}) [8] and are readily soluble in water. Limitations are that they are mainly only used as stains and can be sensitive to photo bleaching and exhibit a pH–dependent fluorescence.[8] They also have a relatively short-lived excited state with a lifetime in the pico to nanoseconds range. Their absorption and emission can be broad with bandwidths in the order of tens of nm, and they usually possess a small Stokes shift between their absorption and emission, which can lead to interference from light scattering in biological media. [8]

Due to the drawback of these different classes of optical probes for biological spectroscopy and bio-imaging, there is therefore a need for a new and better class of optical probes. This would not necessarily replace the current selections, but complement the beneficial properties associated with QDs, fluorescent proteins and organic chromophores. A great deal of effort has therefore been directed towards the design of functionalised emissive Ln^{3+} complexes as optical probes for PL spectroscopy and microscopy. As mentioned previously, Ln^{3+} complexes possess many attractive spectroscopic features that make them very powerful as PL probes for cell imaging. The properties of Ln^{3+} complexes, which also includes the long-lived PL, allows for time-gated detection microscopy that constitutes a very effective way of discriminating background signals from autofluorescence as these are typically processed in the pico to nano second time range.

Autofluorescence is the natural emission of light by biological structures such as mitochondria and lysosomes when they have absorbed light. This can be particularly problematic if UV excitation is used with for instance proteins with

tryptophan residues. NADPH, FADs and flavins will cause auto fluorescence. It is therefore necessary to distinguish the fluorescence originating from inherent fluorophores to the emission of the inserted optical probe.[30]

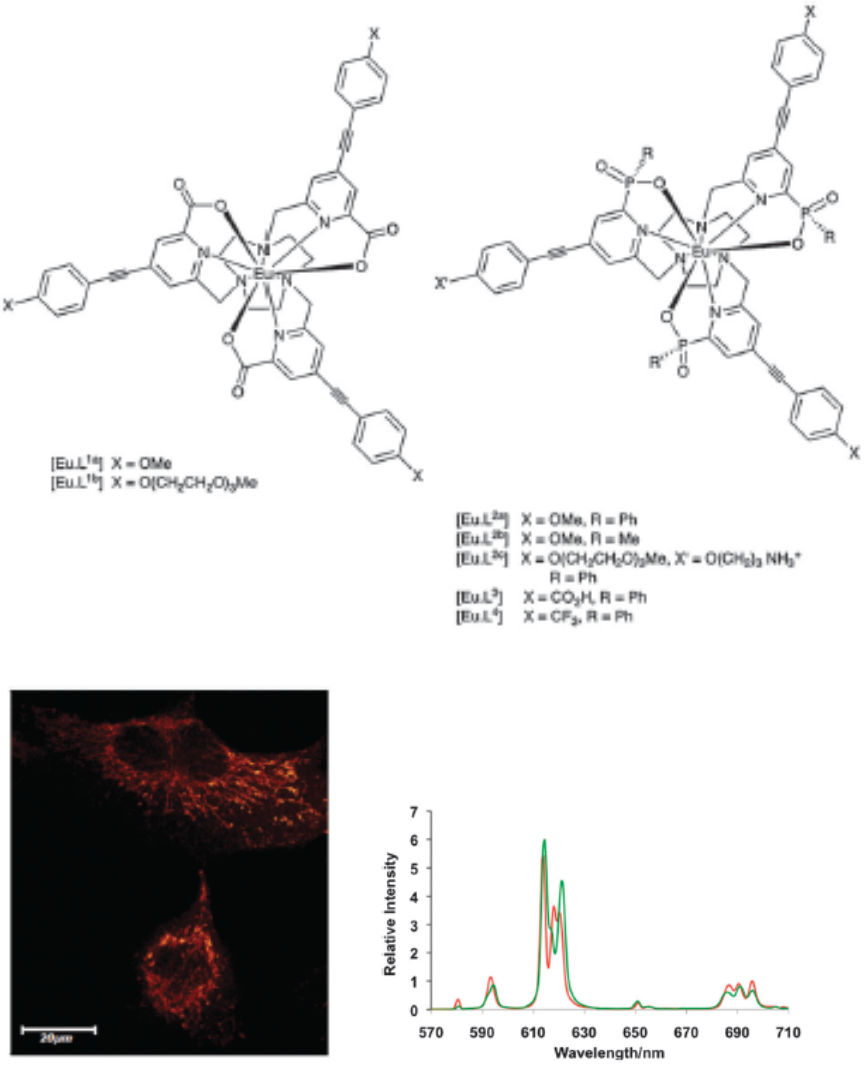

Fig. 1.6 (Top) Molecular structure of Eu^{3+} complex based on triazacyclononane (120 K) showing part of the hydration sphere. (Bottom left microscopy images (Leica SP5 II) showing staining of cellular mitochondria in NIH 3T3 cells for (Eu-L^{2b}) (10Mm, 15 min loading time, $\lambda_{exc\ 355\ nm}$. (Bottom right) Eu^{3+} emission spectra of (Eu-L^{1a}) (green) and (Eu-L^{2b}) (295 K, H_2O, λ_{exc} 355 nm), changes in $\Delta J = 2$ manifold around 615 nm is associated with variation of oxygen donor polarisability. [30]

1.8 Introduction to Anion Sensing.

Anions play a crucial role in many cellular processes including kidney function, intracellular pH homeostasis and sperm maturation.[31] A part of this thesis shows some attempts to study anions with functionalised Ln^{3+} complex using CPL spectroscopy. Due to their exceptional photophysical properties, Ln^{3+} ions afford considerable scope in anion sensing for the development of new chemical entities that can be used as analytical or imaging probes as key sensor materials.

There is furthermore a growing consensus that anions serve as important bio-markers for diseases. Lactate and citrate (Figure 1.7) are key metabolites in cell metabolism.[32] For example, lactate is the major product of aerobic glycolysis that characterizes the metabolism of tumour cells. Lactate analysis of serum is important in sports, clinical and experimental medicine. Citrate is a key metabolite in the Krebs cycle of every aerobic cell. Determination of citrate levels is important in clinical conditions and in cell metabolism. Reduced citrate levels in urine have been linked to kidney dysfunction.[32] Citrate levels are also markedly reduced in malignant prostate cancer tissue and have been shown to provide the most consistent characteristic change in the onset and progression of prostate cancer. Hence, citrate represents a significant and much needed biomarker that may provide an accurate, reliable screening method for the non-invasive detection and monitoring of prostate cancer.[32] Elevated levels of uric acid (hyperuricaemia) are commonly associated with gout and renal disease. Patients on chemotherapy for proliferative disease such as lymphoma, leukaemia often exhibit hyperuricaemia and levels must be monitored to avoid kidney damage.[33] Measurements of uric acid in urine and plasma are therefore also an important marker in clinical diagnosis.

Hence, the determination of anions in clinical conditions and in normal cell metabolism is important. They are therefore important target in probe development, as the knowledge of the concentration and distribution of anions in cellular compartments is essential.

Over the last years, Ln^{3+} complexes have been created capable of the selective binding of bicarbonate under physiological conditions. Specifically, bicarbonate binding is characterised by a noticeable increase in the intensity ratio of the $\Delta J = 2$ / $\Delta J = 1$ transitions of Eu^{3+}. This ratiometric method is more appropriate as the intensity of the MD transition is insensitive to changes in coordination sphere,

which is as a result of anion complexion. Such changes allow for a direct analysis as the variations in the intensity ratios can be plotted as a function of added bicarbonate (Figure 1.8). In the past several years, there has also been growing interest in the CPL active materials where Maeda *et al* [34] first observed anion-driven CPL enhancement response behaviour of chiral BINOL-based boron hybrid complexes.

Anion	Extracellular fluid	Intracellular fluid	Cerebrospinal fluid
Citrate	0.1-0.3	2-4	0.05-0.25
Carbonate	24-27	10-12	20-23
Lactate	0.6-2.3	3-22	0.5-2.2

Table 1: Typical concentration ranges (mM) of selected anions in humans (intracellular values vary considerably with cell type). [32]

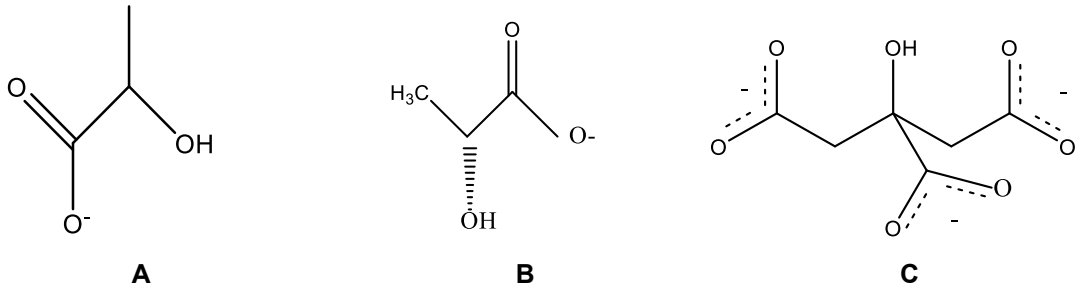

Figure 1.7: **A**: L-lactate, **B**: D-lactate, **C**: Citrate

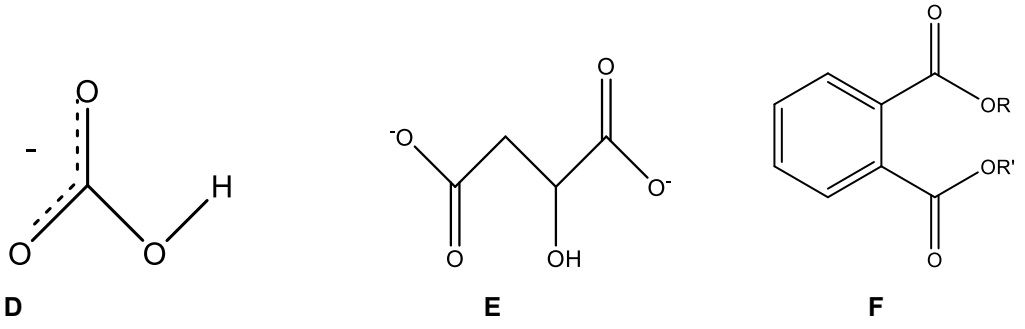

Figure 1.8: **D**: Bicarbonate, **E**: Malate, **F**: Phthalate

1.9 Target of the project.

The work is pursued in order to break new grounds in the study of biological systems using optical spectroscopy, leading to the development of polarised optical luminescence microscopy methods. It is based on the use of the highly luminescent Ln^{3+} complexes, mainly Eu^{3+} and Tb^{3+} complexes, which are the two most commonly used Ln^{3+} ions in bio-imaging and bio-spectroscopy. Ln^{3+} complexes are used in this project because of the exceptional photo-physical properties they possess. Ln^{3+} complexes can be chiral and therefore produce CPL and their interaction with intra-cellular chiral species in cells will modulate the CPL of the Ln^{3+} complex accordingly.

In this work some different Ln^{3+} complexes have been studied with CPL spectroscopy. One aspect that has been investigated in this context is the relationship between complex conformation and the optical CPL signal these will produce. Another part of this work has been focused on the interaction between Ln^{3+} complexes and chiral materials such as some selected anions. In this context the issue is how these interactions may modulate the PL and the CPL of the Ln^{3+} complex.

The microscopic technique development will be achieved by modifying a fluorescence microscope to facilitate measurements of the CP of light. The microscope selected for the project is the confocal system, Leica TCS SP5 II. The need for confocal detection is motivated by the desire to monitor emission processes with high resolution enabling specific binding interactions between optical probes and the chiral target to be studied in intra cellular compartments. The high resolution in confocal microscopy is achieved using the pinhole concept (Figure 1.6). By having a confocal pinhole, the microscope is efficient at rejecting out of focus fluorescent light. Hence, the image comes from a thin section of the sample. By scanning many thin sections through the sample, a 3D image of the sample can be acquired.

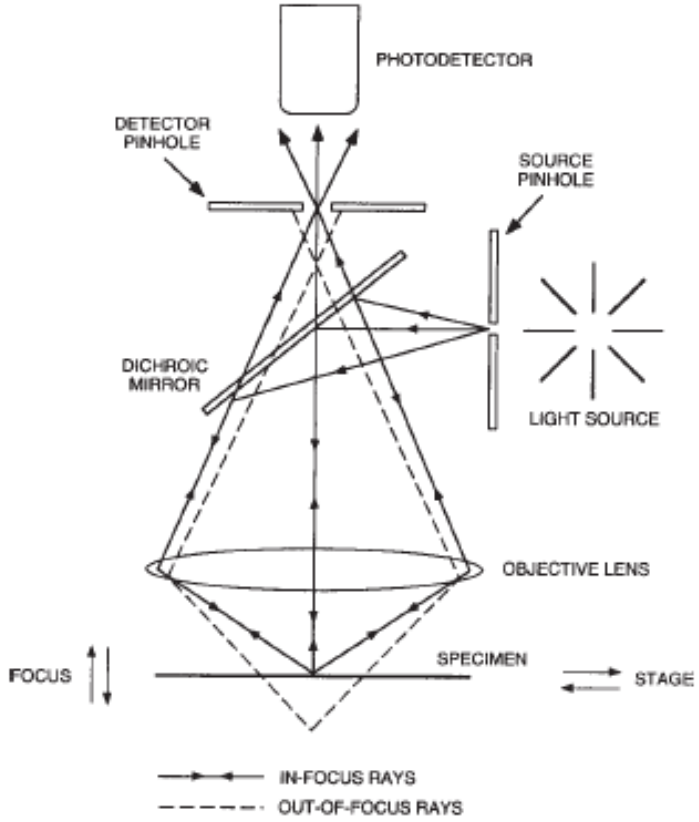

Figure 1.9 Schematic diagram of a confocal microscope illustrating the pinhole concept.[35]

Besides the high resolution and the excellent imaging capabilities of the Leica microscope, other advantages of using this platform is the ability to modify the microscope to make possible the detection of the CPL. The detection of CPL will be achieved by incorporating a PEM into one of the emission pathways of the microscope. The PEM is an optical element used to modulate the polarisation direction and the separation of left and right hand circularly polarised light. Hence it is one of the key components that is required for the purpose of the detection of CPL. An external detector APD connected to the X1 port of the microscope, will be used to acquire CPL signal. A LIA shall be used in conjunction with the PEM to extract the signal from the noise and measure the CPL signals. The signal shall then be fed back into the scanning system of the microscope thereby facilitating an analysis of CPL images of functionalised Ln^{3+} complexes vs conventional PL microscopy images. Ln^{3+} complexes will also be analysed in this work for the sensing of specific anions.

1.10 References.

1. S. Cotton*, Lanthanide and Actinide Chemistry*, Wiley, England, 2006.
2. J. G. Bunzil and C. Piguet; *Taking advantage of luminescent lanthanide ions,* Chem. Soc. Rev., 2005, **34**, 1048-1077.
3. D. F. Shriver, P. W. Atkins and C. H. Langford, *Inorganic Chemistry*, Germany, 2nd edition., 2001.
4. L. M. Bushby, PhD Thesis, Durham Universty, 2001.
5. A. K. Levine, C. F. Palilla, *A new, highly efficient red-emitting cathodoluminescent phosphor (YVO4:Eu) for color television*, Applied Physics Letters, 1964, **5**, 118.
6. N. P. Barnes, *Lanthanide series lasers—near infrared. Handbook of Laser Technology and Applications*, 2003, **3**, 383 -410.
7. J. S. Stefaan, J. V. Greetje, K. Ashwini, H. Uwe, C. M. De. *Magnetoliposomes as magnetic resonance imaging contrast agents, Nanomed Nanobiotechnol*; 2011, **3**, 197-211.
8. S. Pandya, J. Yu and D. Parker, *Engineering emissive europium and terbium complexes for molecular imaging and sensing;* Dalton Trans., 2006, **23**, 2757-2766.
9. I. Nasso, S. Bedel, C. Galaup, and C. Picard; *A Water-Stable and Strongly Luminescent Terbium(III) Macrocyclic Complex Incorporating an Intracyclic Pyrazolylpyridine Chromophore* Eur. J. Inorg. Chem., 2008, **2008**, 2064-2074.
10. Introduction to ratiometric Lanthanide sensors,http://www.fscanltd.com/2.html, (accessed January 18).
11. E. J. New, D. Parker and R. D. Peacock, *Comparative study of the constitution and chiroptical properties of emissive terbium and europium complexes with a common tetraazatriphenylene sensitiser; the nature of the sensitiser determines quenching sensitivity and cellular uptake*, Dalton Trans., 2009, **4**, 672–679.
12. S. Lis, M. Elbanowski, B. Makowska, Z. Hnatejko; *Energy transfer in solution of lanthanide complexes,* Journal of Photochemistry and Photobiology A: Chemistry, 2002, **150**, 233–247.
13. L. M. Bushby, PhD Thesis, Durham Universty, 2001.

14. G. Zucchi, R. Scopelliti, P. A. Pittet, J. C. Bunzli, R. D. Rogers, *Structural and photophysical behaviour of lanthanide complexes with a tetraazacyclododecane featuring carbomoyl pendant arms*, J. Chem. Soc., 1999, 931-938.
15. R. Haner, J. Hall, G. Rihs, Synthesis and Structure of a Macrocyclic Europium Complex and its possible role as a catalyst for phosphodiester transesterification, Helvetica Chimica., 1997, **80**, 487- 494.
16. R. S. Dickins, J. A. K. Howard, C. L. Maupin, J. M. Moloney, D. Parker, J. P. Riehl, G. Siligardi and J. A. G. Williams, Synthesis, *Time-resolved luminescence, NMR spectroscopy, circular dichroism and circularly polarised luminescence studies of enantiopure macrocyclic lanthanide tetraamide complexes*, Chem. Eur. J., 1999, **5**, 1095-1105.
17. D. Parker, R. S. Dickins, H. Puschmann, C. Crossland, and J. A. K. Howard, *Being Excited by Lanthanide Coordination Complexes: Aqua Species,Chirality, Excited-State Chemistry, and Exchange Dynamics* Chemical Reviews, 2002, **6**, 1977-2010.
18. J. E. Roderiguez-Ubis, M. T. Alonso, O. Juanes, R. Sedano, E. Brunet, *The discovery of a simple ligand based on acetophenone bearing excellent quantum yields for the excitation of Eu^{3+} and Tb^{3+},* 1998, **79**, 121.
19. H. Ozaki, E. Suda, T. Nagano, H. Sawai, *Sensitisation of europium (III) luminescence by DTPA derivatives*, Chem Lett., 2003, **29**, 312-313.
20. F. J. Steemers, W. Verboom, D. N. Reinhoudt, E. B. van der Tol, J. W. Verhoeven, *New sensitiser - modified calixarenes enabing near-uv excitation of complexed luminescent lanthanide ions,* Chem.Soc., 1995, **117**, 9408.
21. S. C. Petoud, S. M. Bünzli, K. J. Raymond, *Stable Lanthanide Luminescence Agents Highly Emissive in Aqueous Solution: Multidentate Hydroxyisophthalamide Complexes of Sm^{3+}, Eu^{3+}, Tb^{3+}, Dy^{3+},* ChemSoc., 2003, **44**, 13324–13325.
22. N. S. Baek, M. Nah, Y. H. Kim, S. Roh, and H. K. Kim, *Efficient Energy Transfer Pathways for the Sensitization of Lanthanide Ions by Luminescent Ligands in Luminescent Lanthanide Complexes,* Chem. Soc. 2004, **25**, 443.
23. S. A. Svarovsky and L. Joshi, *Cancer glycan biomarkers and their detection-past, present and future*, Anal. Methods., 2014, **6**, 3918-3936.

24. X. Michalet, F. F. Pinaud, L. A. Bentolila, TS. Doose,G. Sundaresan, S. S. Gambhir, Weiss*, Quantum Dots for Live Cells, in Vivo Imaging, and Diagnostics Science*, 2005, **307**, 538.
25. R. Dunpall, A. A. Nejo, V. S. Pullabhotla, A. R. Opoku, N. Revaprasadu and A. Shonhai, *An in vitro assessment of the interaction of cadmium selenide quantum dots with DNA, iron and blood platelets*, IUBMB Life., 2012, **64**, 995-1002.
26. A. F. Rausch, L. Murphy, J. A. Gareth Williams, and H. Yersin, *Improving the Performance of Pt(II) Complexes for Blue Light Emission by Enhancing the Molecular Rigidity Inorg. Chem*. 2012, **51**, 312−319.
27. X. Yang, C. Yao and G. Zhou, *Highly Efficient Phosphorescent Materials Based on Platinum Complexes and Their Application in Organic Light-Emitting Devices (OLEDs) Platinum Metals,* Rev., 2013, **57**, 2-16.
28. D. N. Kozhevnikov, V. N. Kozhevnikov, M. Z. Shafikov, A. M. Prokhorov, D. W. Bruce, and J. A. Gareth Williams, *Phosphorescence vs Fluorescence in Cyclometalated Platinum(II) and Iridium(III) Complexes of (Oligo)thienylpyridines* Inorg. Chem. 2011, **50**, 3804– 3815.
29. E. O Danilov, A. A Rachford, S. Goeb, F. N Castellano, *Evolution of the triplet excited state in Pt(II) perylenediimides*, J. Phys. Chem., 2009, **113**, 5763–5768.
30. B. N. Atkinson, A. R. Chatwal, H. V. Lomax, J. W. Walton and J. M. J. Williams**,** *Transamidation of primary amides with amines catalyzed by zirconocene dichloride* Chem. Commun., 2012, **48**, 11626-11628.
31. S. J. Butler and D. Parker, *Anion binding in water at the lanthanide centres: from structure and selectivity to signalling and sensing*, Chem. Soc. Rev., 2013, **42**, 1652-1666.
32. R. Pal, D. Parker and L. C. Costello, *A europium luminescence assay of lactate and citrate in biological fluids;* Org. Biomol. Chem., 2009, **7**, 1525-1528.
33. R. A. Poole, F. Kielar, S. L. Richardson, P. A. Stenson and D. Parker, *A ratiometric and non-enzymatic luminescence assay for uric acid: differential quenching of lanthanide excited states by anti-oxidants*, Chem. Commun., 2006, **46**, 4084–4086.

34. H. Maeda, Y. Bando, K. Shimomura, I. Yamada, M. Naito, K. Nobusawa, H. Tsumatori and T. Kawai, *Chemical-Stimuli-Controllable Circularly Polarized Luminescence from Anion-Responsive π-Conjugated Molecules* J. Am. Chem. Soc., 2011, **133**, 9266–9269.
35. S. W. Paddock, *Principles and practices of laser scanning confocal microscopy*. Molecular Biotechnology, 2000, **16**, 127-149.

2 THEORY OF LANTHANIDE IONS (Eu^{3+} and Tb^{3+}).

2.1 Electronic Structure of Lanthanide ions.

The Ln^{3+} ions in their ground state configuration contain the closed shell electronic structure of the noble gas xenon, and have 2 or 3 external electrons ($6s^2$ / $5d\ 6s^2$), in addition to their complement of $4f^n$ electrons.

$$1s^2\ 2s^2\ 2p^6\ 3s^2\ 3p^6\ 3d^{10}\ 4s^2\ 4p^6\ 4d^{10}\ 5s^2\ 5p^6 = \{Xe\}$$

Z	Element	Symbol	Atom	M^{3+}	M^{3+} radius(Å)
57	Lanthanum	La	$[Xe]5d^16s^2$	[Xe]	1.061
58	Cerium	Ce	$[Xe]4f^15d^16s^2$	$[Xe]4f^1$	1.034
59	Praseodymium	Pr	$[Xe]4f^36s^2$	$[Xe]4f^2$	1.013
60	Neodymium	Nd	$[Xe]4f^46s^2$	$[Xe]4f^3$	0.995
61	Promethium	Pm	$[Xe]4f^56s^2$	$[Xe]4f^4$	0.979
62	Samarium	Sm	$[Xe]4f^66s^2$	$[Xe]4f^5$	0.964
63	Europium	Eu	$[Xe]4f^76s^2$	$[Xe]4f^6$	0.950
64	Gadolinium	Gd	$[Xe]4f^75d^16s^2$	$[Xe]4f^7$	0.938
65	Terbium	Tb	$[Xe]4f^96s^2$	$[Xe]4f^8$	0.923
66	Dysprosium	Dy	$[Xe]4f^{10}6s^2$	$[Xe]4f^9$	0.908
67	Holmium	Ho	$[Xe]4f^{11}6s^2$	$[Xe]4f^{10}$	0.899
68	Erbium	Er	$[Xe]4f^{12}6s^2$	$[Xe]4f^{11}$	0.881
69	Thulium	Tm	$[Xe]4f^{13}6s^2$	$[Xe]4f^{12}$	0.869
70	Ytterbium	Yb	$[Xe]4f^{14}6s^2$	$[Xe]4f^{13}$	0.858
71	Lutetium	Lu	$[Xe]4f^{14}5d^16s^2$	$[Xe]4f^{14}$	0.848

Table 2.1: Electronic configuration of lanthanide atoms and trivalent ions with the radii of the trivalent ions.[1]

2.2 Term Symbol.

The distribution of the electrons around the nucleus of a Ln^{3+} ion can be described by a wave function that is specified by four quantum numbers, *n, L, S* and *J*. The electronic structure of Ln^{3+} ions is denoted by their term symbol, which is given by $^{2S+1}L_J$. Where *2S+1* is the multiplicity of the state. [2]

S = the spin angular momentum quantum number,
L = the orbital angular momentum quantum number
J = represents the spin-orbit coupling quantum number.
n = principle quantum number

As mentioned previously, Ln^{3+} are characterised by their partially filled 4*f* shells, which are shielded from its surroundings by the 5*s* and 5*p* shells. The electron configuration in the 4*f* orbitals give rise to different energy levels due to the specific interactions occurring within the shell. The first interaction is the columbic interaction, which represents electron-electron repulsion within the 4*f* orbitals. It is also the strongest of all the interactions, which separates the configuration of the 4*f* into ^{2S+1}L manifold. The ^{2S+1}L manifold is then split by spin orbit coupling yielding the electronic energy levels (J) described by the term symbols shown in figure 2. For instance, for Eu^{3+}, $4f^6$, the largest multiplicity is obtained when each electron is associated with a unique 4f wave function: $S = 6 \times ½ = 3$; therefore, (2S + 1) = 7. To obtain the largest orbital multiplicity, these electrons have to be related with wave functions having the largest m_ℓ values, i.e., +3, +2, +1, 0, –1, and –2; the sum is 3, henceforth *L* = 3 and *L* = F: the ground term is a spin septet, ^7F with overall multiplicity $7 \times 7 = 49$. And For Tb^{3+}, electronic configuration is $4f^8$. $S = 8 \times ½ = 4$; therefore, (2S + 1) = 9. m_ℓ values is; +4,+3, +2, +1, 0, –1, –2, -3 and -4; the sum is 3, henceforth *L* = 3 and *L* = F: the ground term is a spin septet, ^7F.

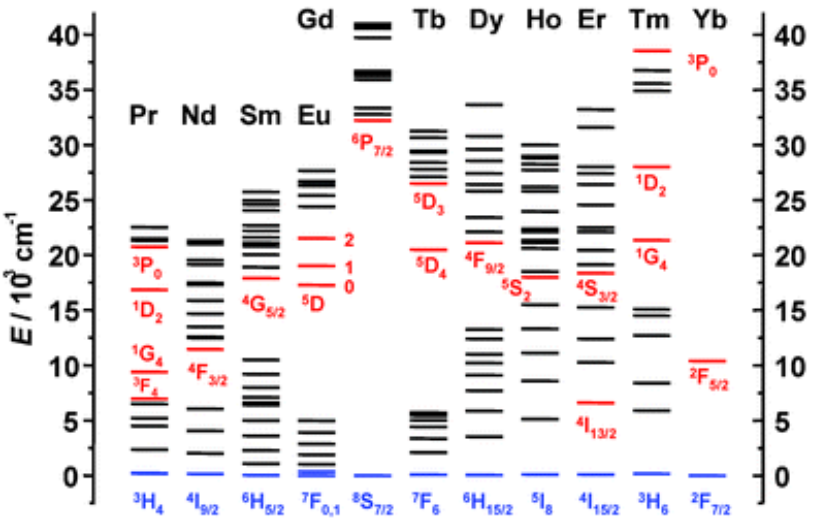

Figure 2.2 Partial energy diagram for the emissive lanthanide ions (red lines indicates the main emissive levels, and blue lines indicate the ground state.[3]

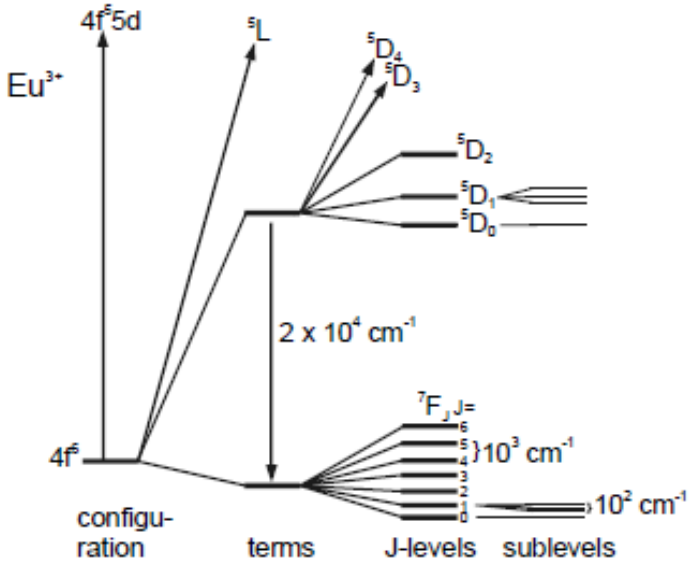

Figure 2.3 Splitting of the 4f energy levels of Eu^{3+}. [4]

Generally, atomic spectra obey the following rules;

- $\Delta S = 0$. This spin selection rule forbids electronic transitions between levels with different spin states. However in the case of Ln^{3+} the $\Delta S \neq 0$ transitions are allowed.

- ΔL = 0, ±1, with Δl = ±1, the orbital angular momentum of an individual electron must change during the transition.
- ΔJ = 0, ±1, but J = 0 to J = 0 is forbidden.
- The parity selection rule forbids electronic (electric-dipole) transitions between levels with the same parity. An example is the f-f transitions.

The two processes by which the 4*f*-4*f* transitions of Ln^{3+} complexes can obtain intensity are by MD and induced ED. The final level of splitting where the J-levels are split by crystal field effect is also an important splitting pattern. This splitting appears as fine structure on the individual bands and may be used to provide information about the symmetry of the coordination environment.

There is a number of Ln^{3+} ions that are emissive, but the intensity, i.e. the PLQY is in many cases relatively low, which makes these systems less useful in the context of biological spectroscopy and biological imaging. Furthermore, there are issues with excitation and emission wavelengths that also render many Ln^{3+} ions and complexes thereof less useful. The exceptions are the Eu^{3+} and Tb^{3+} ions, which, in complexes, can produce intensive (high PLQY) PL in the optical/visible wavelength range. Furthermore, these ions are relatively easy to optically excite using wavelengths in the UV-blue range, which is slightly beyond the absorption of many natural systems/chromophores that produces auto fluorescence in more complex biological systems.

2.3 Eu^{3+} Emission Spectral Features

The emission spectrum of Eu^{3+} provides an excellent illustration of the features of Ln^{3+} spectra. The bands comprise of pure MD, ED and entirely forbidden transitions. The theory of ED transitions [5] yields a selection rule in case the initial level has $J = 0$; transitions to levels with uneven J are forbidden. In addition, the $J = 0$ $J = 0$ transition is forbidden, because the orbital momentum does not change. This restricts the spectrum to the $^5D_0 \rightarrow {}^7F_1$ (ΔJ = 1) at 590 nm, a MD transition, the $^5D_0 \rightarrow {}^7F_2$ (ΔJ = 2) at 612 nm is hypersensitive induced ED emission band and extremely sensitive to the symmetry of the coordination sphere. The $^5D_0 \rightarrow {}^7F_4$ (ΔJ = 4) at 700 nm is a weak induced ED emission. The transitions ΔJ = 0, 3 and 5 are forbidden by both MD and ED schemes and if they are observed, they are said to "borrow" their intensity from

the ΔJ = 2 transition through a j - j mixing mechanism. Studying the emission spectra of Eu^{3+} complexes can provide useful information on the symmetry and structural nature of the coordinating environment around the ion. Several authors now use the recognised method of the ratio of intensity of the ΔJ = 2 transition to ΔJ = 1 transition as being a measure of the degree of symmetry in the electric field surrounding the ion. In centrosymmetric environments, the MD ΔJ = 1 transition is the most intense. In asymmetric environments the hypersensitive ED ΔJ = 2 transition of Eu^{3+} dominates, and can be increased many times. This information is mainly acquired from the splitting associated with a particular band. Since both the $^5D_0$ and $^7F_0$ states in Eu^{3+} are degenerate [6], every independent Eu^{3+} environment will have a unique ΔJ = 0 band. Thus, if any splitting is observed in the $^5D_0 \rightarrow {}^7F_o$ transition in Eu^{3+}, it therefore means that there is more than one Eu^{3+} site although if there is no splitting observed, this does not necessarily indicate a single Eu^{3+} site. Splitting in ΔJ = I, 2, 7 for one individual Eu^{3+} site can at most give three separate components, and the presence of more than 5 components in the ΔJ = 2 band is also indicative of more than one Eu^{3+} site by the rule 2J + 1. A relatively intense ΔJ = 0 band indicates that the Eu^{3+} ion experiences a strong linear crystal field component.[7]

2.4 Tb^{3+} Emission Spectral Features.

The Tb^{3+} ion is characterised by emission from the $^5D_4$ state. The PL emission arises from the following transitions. The $^5D_4 \rightarrow {}^7F_5$ (ΔJ = 1) at 545 nm is hypersensitive but not as sensitive as the Eu^{3+} ΔJ = 2 transition. In addition, the ΔJ = 1 at ~645 is generally also observed. The spectra does not provide much information about the local symmetry of the metal ion because the J values of the levels involved in the transitions are high resulting in splitting of the J-levels into many sub-levels. The PL transitions of Eu^{3+} and Tb^{3+} are also shown in figure 2.4.

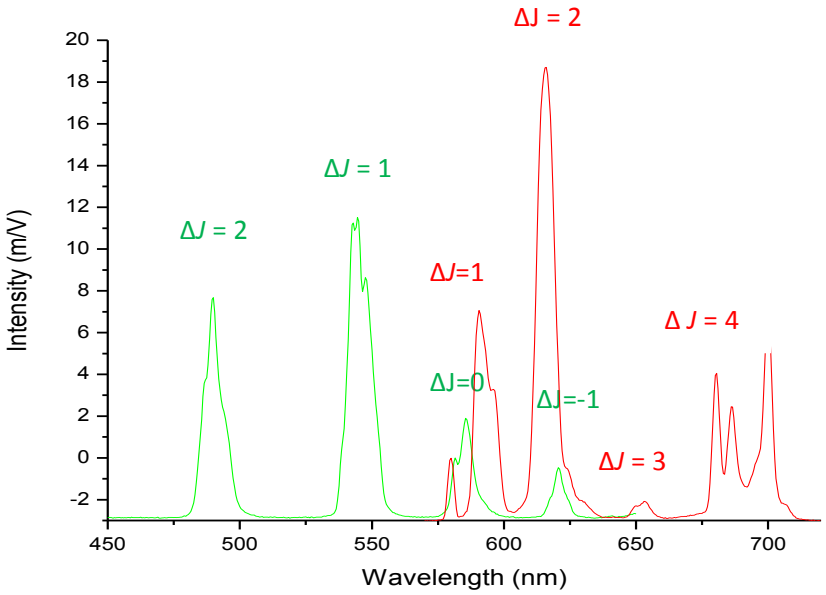

Figure 2.4 PL spectra of Eu^{3+} (red) and Tb^{3+} (green) showing the different emission transitions. These are measured using the CPL spectrometer used in this work. See chapter 3 for experimental details.

2.5 Sensitisation of the Ln^{3+} ion.

Ln^{3+} ions possess low molecular absorption coefficients (< 3 M^{-1} cm^{-1}) [8], which is a major drawback for direct excitation. In order to overcome this problem, the sensitiser, which has a large molecular absorption coefficient, (10^5 – 10^6 M^{-1} cm^{-1}) is covalently attached to the Ln^{3+} complex to allow indirect excitation of the Ln^{3+} complex via intermolecular EET. Upon optical excitation the sensitiser is promoted to the singlet excited state (S_1). At this point, the S_1 excited state can undergo either a non-radiative decay through IC or a radiative decay through fluorescence ($S_1 \rightarrow S_0$). Most importantly in this context is a third pathway, which is ISC to populate the triplet state ($S_1 \rightarrow T_1$). In this process the spin multiplicity of the senstiser is altered in the transition which in turn results in the long-lived meta stable triplet state T_1. In the triplet state, the sensitiser phosphorescence ($T_1 \rightarrow S_0$) competes with EET to the Ln^{3+} ion. For a system with efficient EET there should therefore be no observable phosphorescence or fluorescence from the sentiser. Instead, the emission should originate exclusively from the Ln^{3+} ion. The Jablonski diagram (Figure 2.5) shows the combined photo physical system of the sensitising chromophore and the emissive Ln^{3+} complex.

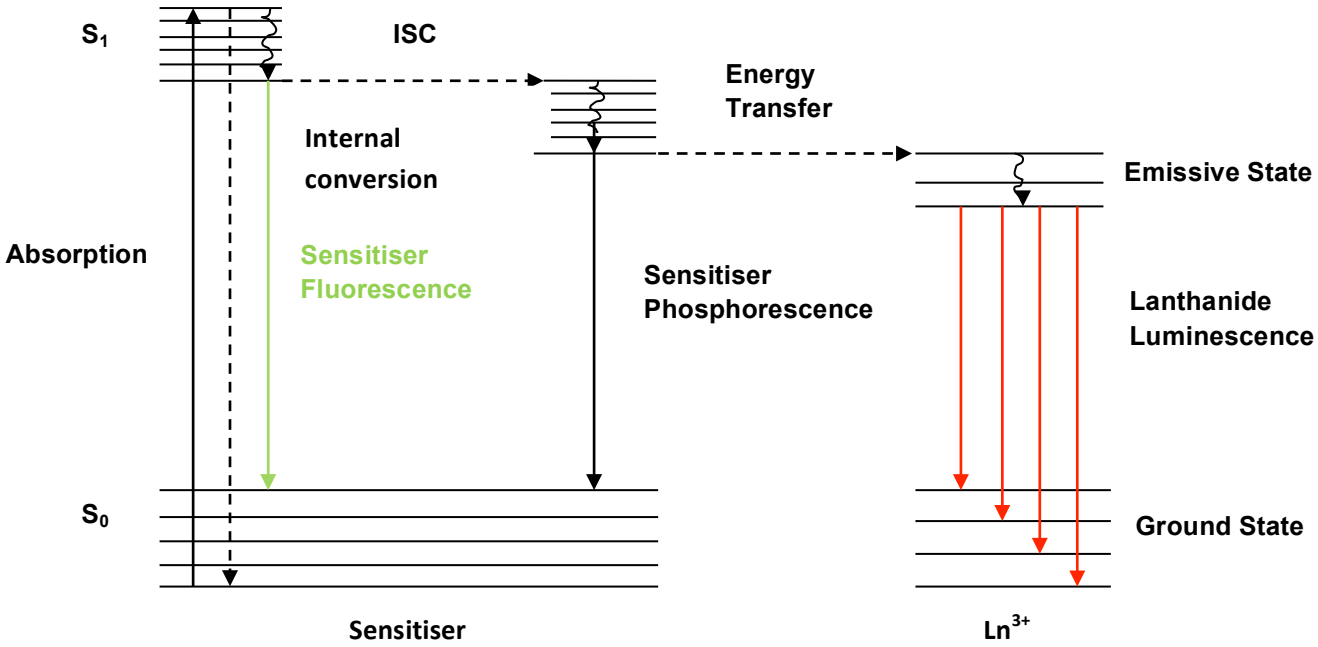

Figure 2.5 Jablonski diagram showing excitation energy transfer from the triplet state of the antenna chromophore into the ^5D_J manifold of Ln^{3+} ions such as Eu^{3+} or Tb^{3+}.

Hence, the overall PLQY (Φ_{tot}) of the complex upon excitation of the chromophore is determined by the efficiency of the sensitiser, n_{sens}, and by the Ln^{3+} ion PLQY, Φ_{Ln}. [9]

$$\Phi_{tot} = \eta_{sens}\Phi_{Ln} \qquad (2.1)$$

It has been shown that the process of energy transfer from the T_1 state to the Ln^{3+} emissive state can take place via either a Dexter mechanism or a Förster mechanism.

For effective sensitisation of Eu^{3+} and Tb^{3+} PL, the organic chromophore has to possess some essential physical properties. A high molar extinction coefficient [10] such that the S_1 state is readily populated, a $S_1 - T_1$ energy gap of less than 7000 cm^{-1} is desirable to minimise ligand fluorescence and allow for efficient ISC to populate the T_1 state of the sensitizer with the S_1 preferably lying less than about 29000 cm^{-1} [10] above the ground state S_0. A fast EET process leading to population of the Ln^{3+} excited state is facilitated by selecting the triplet energy level of the sensitizer to lay at least 2,000 cm^{-1} above the emissive Ln^{3+} excited state. If the

distance is too small, activated back energy transfer could occur leading to reduction in emission intensity and lifetime of the Ln^{3+} emission. Other important features include the ability to coordinate to the Ln^{3+} ion to minimize the sensitiser to Ln^{3+} distance. This is not only beneficial for the desired antenna-Ln^{3+} intramolecular energy transfer, but effectively shields the metal ion from intermolecular binding by maximising its coordination requirements. This organisation tends to inhibit the possibility of quenching by electron-transfer.

As mentioned previously, apart from the radiative emission process that occurs from the excited state of the Ln^{3+} complex, non-radiative processes can also take place competing with the desired radiative process. These are generally termed quenching processes. Quenching can result in deactivation of the excited state leading to a reduction of the overall PLQY. Figure 2.6 shows the three excited states that can be deactivated by the quenching process; the sensitiser S_1 and T_1 and the Ln^{3+} emissive state.

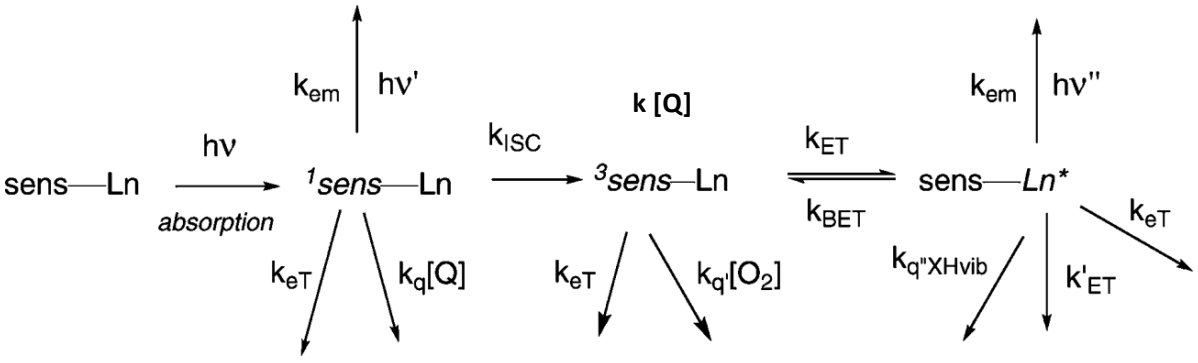

Figure 2.6 Photo physical pathways and quenching processes for sensitised emission of Ln^{3+} ions Eu^{3+} or Tb^{3+}.[11]

The singlet and triplet excited state of the chromophore can be deactivated by various electron, energy and/or vibrational energy transfer processes. A study by Kielar *et al.* [12] showed the possible quenching mechanisms of the three excited states. The S_1 and T_1 states can either undergo fluorescence or phosphorescence respectively or can be deactivated by electron charge transfer "k_{eT}" or deactivation by singlet oxygen formation in the T_1 state. The Ln^{3+} emissive state can also be deactivated by vibrational relaxation "$k_{q"XHvib}$", energy transfer "k'_{ET} to an energy-matched acceptor group and "k_{eT}". Various other studies on the quenching of the Ln^{3+}

emissive state have also been investigated in the past. An important study that was made by Beeby *et al.* [13] showed the effect of OH, NH and CH oscillators on the Ln^{3+} emissive state. They studied Eu^{3+} and Tb^{3+} complexes in H_2O and D_2O and concluded that quenching of the Eu^{3+} excited state by amine NH oscillators is more than twice as efficient as OH quenching and that OH oscillators in bound water molecules are the most effective quenchers in the solid-state and in solution. This is important because for Eu^{3+}, the PL output can be used as a probe for coordination environment to estimate the number of coordinated water molecules and also to obtain information relating to the symmetry of the first coordination sphere. The studies also showed that the radiative lifetime is reduced by the impact of the quencher. The deactivation of the Ln^{3+} emissive state occurs by vibrational energy transfer process involving high-energy vibrations of solvent molecules or of the bound ligand. It also showed that the extent of PL quenching by water molecules is inversely proportional to the energy gap between the emitting state and the ground state and that each oscillator quenched the excited state independently.

2.6 Mechanism of Energy Transfer.

There are two main classes of electronic energy transfer mechanism: radiative and non-radiative. Each process relies on overlap between the emission spectrum of the donor and the absorption spectrum of the acceptor. Radiative energy transfer involves the donor emitting light that is subsequently reabsorbed by the acceptor. This mechanism is favoured where the spectral overlap is good and the PLQY of the donor and the light absorbing properties of the acceptor are maximised. There are a number of different mechanisms that are generally accepted to occur for the non-radiative interaction. In principle, the energy transfer step may occur either from the singlet or triplet excited states of the chromophore. In most cases only the latter is significant, but examples have been postulated of direct energy transfer from the sensitiser's first singlet excited state to the lanthanide emissive state.[14] There are three mechanisms that detail energy transfer from the triplet state of the chromophore to the emissive state of lanthanide: the dipole-dipole pathway (Förster); the exchange mechanism (Dexter); and a dipole-multipole mechanism. The main mechanisms are the former two.

2.6.1 The Förster Mechanism.

The Förster [15] mechanism is a dipole-dipole (coulombic) interaction between the donor (*D*) and acceptor (*A*) and can be expressed as the rate of energy transfer (k_{EET}) which is a function of the separation of the donor and acceptor excited and ground states (R_{DA}) with a distance dependence of R_{DA}^{-6}. Förster showed that for allowed transitions (between the singlet excited states of organic chromophores) k_{EET} is related to the spatial distance between A and D and the donor lifetime, τ_0 in the absence of A:

$$k_{ET} = \frac{1}{\tau_0}\left[\frac{R_{of}}{r}\right]^6 \qquad 2.2$$

R_{of} = the critical distance for energy transfer, defined as the intermolecular separation between donor and acceptor at which $k_{ET} = k_R$ (rate of radiative decay)

$$R_{of} = 8.78\times10^{-2}\cdot\kappa^2\cdot\Phi_D\cdot n^4\cdot J \qquad 2.3$$

κ^2 = orientation factor, which for randomly oriented molecules (for a random mutual orientation of the donor and accepetor chromophores.

Φ_D = the quantum yield of the donor emission in the absence of A

n = the refractive index of the solvent

J = the spectral overlap integral of the absorption spectrum of the acceptor.

The constant in equation 2.3 is a composite constant due Avogadro's number, the refractive index of the medium and a number of conversion factors originating from the derivation of equation 2.3.

Förster also suggested that other terms must be considered when the dipole-dipole interaction is weak because of forbidden optical transitions in D or A. forbidden optical transitions with $\Delta S \neq 0$; if $AS \neq 0$ for $D^* \rightarrow D$ and $AS = 0$ for $A \rightarrow A^*$, then the Förster theory still holds since the slower k_{EET} is compensated by a longer time delay. Where $AS = 0$ for $D^* \rightarrow D$, but $AS \neq 0$ for $A \rightarrow A^*$, energy transfer may only occur over short distances (i.e. Förster forbidden). For symmetry-forbidden transitions,

Förster suggested that energy transfer might be determined by dipole-quadruple interactions with r^{-8} dependence. Indeed k_{EET} through resonance coupling actually has a r^{-n} dependence with n = 6, 8, or 10 for dipole-dipole, dipole-quadropole and quadropole-quadropole interactions respectively.[16]

2.6.2 Dexter Mechanism.

The Dexter [17] mechanism for EET is an electron exchange process that involves a physical overlap between the orbitals of donor (sensitiser) and the acceptor (Ln^{3+} ion). In this process there is an exchange of an electron in the donor excited state and an electron in the Ln^{3+} ion ground state. The mechanism is strongly distance dependent as the energy transfer rate diminishes rapidly at distances larger than a few Å (beyond the van der Waals radius). This is due to the fact that electron densities usually fall off exponentially as the distance from the nucleus increases. Therefore efficient sensitisation requires as small a separation as possible. The rate of EET according to the Dexter mechanism is given by the equation,

$$k_{EET} = C \cdot J \cdot e^{-\frac{2R_{DA}}{L}} \qquad (2.4)$$

Where;

C = a specific orbital interactions constant

J = measure of spectral overlap integral, normalised for the absorption coefficient of the acceptor as given before by equation 2.4

R_{DA} = distance between D and A

L = separation of the donor and acceptor molecules relative to their van der Waals radii

Dexter's mechanism of energy transfer can only occur when the Wigner spin correlation rule is obeyed. This states that if S_i and S_2 are the initial total spins of the electrons in the colliding species (D and A), the resultant total spins of the two systems taken together must have one of the values $|S_1 + S_2|$, $|S1 + S_2 - I|$, $|S_1 + S_2 - 2|$,... $|S_1 - S_2|$. Unlike the Förster theory, which is greatly influenced by J and 4>D, the Dexter theory of energy transfer has normalised values of J, reducing its

significance. Thus, the amount of energy transferred does not significantly depend on the extinction coefficient of the acceptor and therefore it is possible to observe efficient sensitisation of many Ln^{3+} compounds.[17] The proximity of D and A is the crucial parameter in Dexter energy transfer, and the properties of A and D themselves (the transition dipole moments, and the spectral overlap of D emission and A absorption) as well as the spatial distance are important parameters in Forster energy transfer.

2.7 CPL Spectroscopy of Ln^{3+} Complexes.

CPL spectroscopy involves the detection of differential emission of left and right circularly polarised (CP) light and is referred to as the emission analogue of circular dichroism (CD). In the case of CD, the electronic ground state is being investigated, while in CPL, the electronic excited state is monitored. Hence, CD is the difference in absorption of left and right CP light.

$$CD = A_L - A_R \tag{2.5}$$

In CPL the differential intensity is measured and the CPL is therefore proportional to this difference,

$$CPL \propto I_L - I_R \tag{2.6}$$

CPL experiments produce two measurable quantities, the total intensity, $I(\lambda)$ and the emission circular intensity differential $\Delta I(\lambda)$, both being a function of wavelength. These values are obtained in arbitrary units depending on the experimental layout but these are directly related to the CP condition of the PL. The total PL intensity is defined as equation 2.7.

$$I(\lambda) = I_L(\lambda) + I_R(\lambda) \tag{2.7}$$

The CPL differential is defined as:

$$\Delta I(\lambda) = I_L(\lambda) - I_R(\lambda) \tag{2.8}$$

Where $I_L(\lambda)$ and $I_R(\lambda)$ represents the intensities of left (L) and right (R) handed CP components of emitted PL, respectively. The degree of polarisation is measured by the dissymmetry factor [18] (g_{em}), which is defined by equation (2.9).

$$g_{em}(\lambda) = \frac{2\Delta I(\lambda)}{I(\lambda)} \tag{2.9}$$

The quantities contained in the equation above (2.9) are the macroscopic observables of the CPL measurement. However, these depend on the microscopic molecular properties of the chromophore that produces the CPL.

For both CD and CPL the intensity depends on the presence of an ED transition in conjunction with a MD transition, leading to optical rotation. The quantum mechanical theory of optical rotation was first derived by Rosenfeld who derived the formalism for the interaction between electromagnetic radiation (optical) and molecular systems in this context. The sign and magnitude of the optical rotation R_{ge} is associated with a transition $\psi_g \rightarrow \psi_e$ (where g is the ground state and e is the excited state) which is governed by the rotatory strength R_{ge}(Rosenfeld equation), [18]

$$R_{ge} = imag(\langle \psi_g | \overline{\mu} | \psi_e \rangle \times \langle \psi_g | \overline{m} | \psi_e \rangle) \tag{2.10}$$

where $\overline{\mu}$ represents the ED transition vector and $\overline{m}$ represents the MD transition vector. $\langle \psi_g |$ and $| \psi_e \rangle$ represents the states as previously defined. The polarisation of the PL emission is quantified by the g_{em} factor for the microscopic origin and can subsequently be written as equation 2.11

$$g_{em} = \frac{4R_{ge}}{|\overline{\mu}_{ge}|^2} \tag{2.11}$$

Assuming the angle between ED transition moment and the MD transition moment is θ, the rotatory strength will also have an orientational dependence on θ as:

$$R_{ge} = \left|\bar{m}_{ge}\right|\left|\bar{\mu}_{ge}\right|\cos\theta \tag{2.12}$$

For a given transition, g_{em} is constant where the CPL emission and total PL emission have identical line shapes. Replacing the rotational strength in equation 2.11 with equation 2.12 shows that the CPL intensity contained in the dissymmetry factor g_{em} scales with the MD transition as,

$$g_{em} = \frac{4\left|\bar{m}_{ge}\right|}{\left|\bar{\mu}_{ge}\right|}\cos\theta \tag{2.13}$$

In order for an electronic transition to possess a CPL signal, i.e g_{em} is greater than 0, it therefore requires that $\bar{m}_{ge} \neq 0$. For chiral systems such as Ln^{3+} complexes, this is an intrinsic property mainly due to the presence of a metal centre. Hence CPL may be observed in the absence of any externally applied force fields. CPL is suited to studies of the chirality of Ln^{3+} complexes also because the emissive Ln^{3+} ion acts as a pure spherical emitter therefore avoiding issues of anisotropy. Ln^{3+} complexes possess high g_{em} values. eg Eu^{3+} and Tb^{3+} complexes possess g_{em} values between 0.1-0.5 (theoretical maximum of g_{em} being 2)[18] compared to organic materials, which are typically in the range about 10^{-3} - 10^{-4} *(*g_{em} = *2* for 100% CPL light*)*.

2.8 Characteristics of Circularly Polarised Light.

CP light describes a rotation of the electric field vector around the direction of propagation. When considering polarisation, only the electric field vector is described since the magnetic field is perpendicular to the electric field and proportional to it. Figure 2.7 shows a wave of linearly polarised light propagating along the z-axis which contains electric field vectors of polarised light whose directions are mapped in the x and y plane. Equation 2.13 describes the two different components mapped on the x and y axis accordingly.

$$\bar{E}_x(z,t) = \bar{i}E_{0_x}\cos(kz-\omega t)$$
$$\bar{E}_y(z,t) = \bar{j}E_{0_y}\cos(kz-\omega t-\zeta) \qquad (2.14)$$

where ζ is the phase difference, ω is the angular frequency of light, $\bar{E}_{0_x}$ is the amplitude along x and $\bar{E}_{0_y}$ is corresponding amplitude along y and k is the propagation direction.

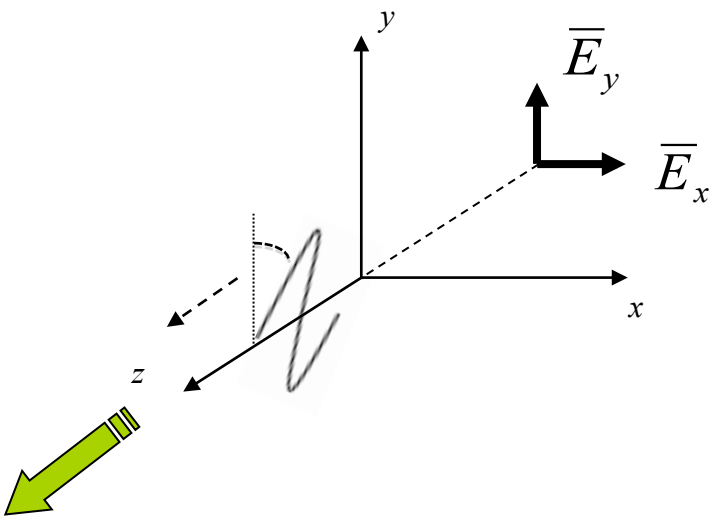

Figure 2.7: A wave of light propagating along the z axis with electric field vectors of linearly polarised light whose directions are mapped in the x and x planes.

As with any vector quantity, the electric field vector describing the polarisation condition can be resolved into projections along the x and y axis. For linearly polarised light the phase difference will be constant during the propagation process unless passage through an anisotropic medium takes place. Hence, the total linearly polarised light can be described as a superposition of the two projections previously given by equation (2.13)

$$\bar{E}(z,t) = \bar{E}_x(z,t) + \bar{E}_y(z,t) \tag{2.15}$$

Depending on the values of $\bar{E}_{o_x}$, $\bar{E}_{o_y}$, ζ, the superposition can result in linear polarisation, elliptical polarisation or circular polarization.

If $\bar{E}_{o_x} = \bar{E}_{o_y} = \bar{E}_o$, i.e. the amplitude of the two contributions are similar, and the phase difference is $\zeta = \frac{\pi}{2}$, the resultant wave is CP light. Hence, CP light is generated from the sum of two linearly polarised waves, and this result in the following fundamental equation, which describes the propagation of CP light.

$$\bar{E}(z,t) = E_0 \left[\bar{i} \cos(kz - \omega t) + \bar{j} \sin(kz - \omega t) \right] \tag{2.16}$$

However, this equation only describes one rotation direction. In reality the opposite rotation direction is also possible and therefore equation 2.16 [18] can be divided up into a sum of two different contributions,

$$\bar{E}_R(z,t) = \frac{E_0}{2} \left[\bar{i} \cos(k_R z - \omega t) + \bar{j} \sin(k_R z - \omega t) \right] \tag{2.17}$$

$$\bar{E}_L(z,t) = \frac{E_0}{2} \left[\bar{i} \cos(k_L z - \omega t) - \bar{j} \sin(k_L z - \omega t) \right] \tag{2.18}$$

where equation 2.18 represents right handed CP light and equation 2.19 represents left handed CP light. The PL of chiral functionalised Ln^{3+} complexes is described by these two fundamental equations.

2.9 References.

1. Electronic configuration and position in periodic table, Chemistry, http://www.expertsmind.com/questions/electronic-configuration-and-position-in-periodic-table-30189108.aspx, (accessed January 2015).
2. P.W Atkins, *Physical Chemistry*, Oxford University Press, Oxford, 1988, 2nd edn., 1095.
3. D. Parker, *Luminescent lanthanide sensors for pH, pO2 and selected anions*; Coord. Chem. Rev., 2000, **205**, 109.
4. J. G. Bunzli, *The europium(III) ion as a spectroscopic probe in bioinorganic chemistry*, *Inorg. Chim. Acta,* 1987, **139***,* 219.
5. B. R. Judd, *Optical absorption intensities of rare-earth ions*, *Phys. Rev.,* 1962,***127****,* 750.
6. A. K. Parchura and R. S. Ningthoujam, *Behaviour of electric and magnetic dipole transitions of* Eu^{3+} $^5D_0$ *A* $^7F_0$ *and Eu–O charge transfer band in Li+ co doped YPO4:*Eu^{3+}. RSC Adv., 2012, **2**, 10859–10868.
7. G. Blasse, A. Bril, On the Eu^{3+} ;*Fluorescence in mixed metal oxides II. The* ^7Fo *emission, Philips Res. Repts.,* 1966**, 21**, 368.
8. J. G. Bünzli and C. Piguet, *Taking advantage of luminescent lanthanide ions*, Chem. Soc. Rev, 2005, **34**, 1048-1077.
9. M. H.V. Werts, *Making sense of Lanthanide luminescence;* Science progress 2005, **88(2)**, 101-131.
10. S. Pandya, J. Yu and D. Parker, *Engineering emissive europium and terbium complexes for molecular imaging and sensing,* Dalton Trans., 2006, **23**, 2757-2766.
11. R. A. Poole, G. Bobba, M. J. Cann, J. Frias, D. Parker and R. D. Peacock, Synthesis and characterisation of highly emissive and kinetically stable lanthanide complexes suitable for usage 'in cellulo', Org. Biomol. Chem., 2005, **3**, 1013-1024.
12. F. Kielar, C. P. Montgomery, E. J. New, D. Parker, R. A. Poole, S. L. Richardson and P. A. Stenson, *A mechanistic study of the dynamic quenching of the excited state of europium(III) and terbium(III) macrocyclic complexes by charge- or electron transfer.* Org.Biomol.Chem., 2007, **5**, 2975.

13. A. Beeby, D. Parker, J. A. G. Williams, *Photochemical investigations of functionalised 1,4,7,10-tetraazacyclododecane ligands incorporating naphthyl chromophores,* J. Chem. Soc. Perkin Trans., 1996, **2**, 1565-1579.
14. A. Brown, F. Wilkinson, *Intermolecular energy transfer in rigid matrices at 77 K. Part 1. Quenching of triphenylene phosphorescence by aquated terpositive lanthanide ions,* J. Chem. Soc, Faraday Trans., 1979, **75**, 880.
15. T. Forster, *Transfer mechanisms of electronic excitation (10th Spiers Memorial Lecture), Discuss. Faraday Soc.,* 1955, ***27****, 1.*
16. G. E. Buono-Core, H. Li and B. Marciniak, Quenching of excited states by lanthanide ions and chelates in solution, Coord. Chem. Rev., 1990, **99**, 55-87.
17. D. L. Dexter, *A theory of sensitised luminescence in solids*, J. Chem. Phys., 1953, **21**, 836.
18. E. Hecht, *Optics,* Addison Wesley Freeport , New York, *1998,* 3rd edn, 1998.

3. EXPERIMENTAL

3.1 Method

The PL spectra and CPL spectra were recorded using a laboratory made CPL spectrometer. As discussed previously in chapter 2.7, the basic aim of CPL spectroscopy is to determine the difference in intensity between the left and right-handed CP emissions as a function of wavelength. This was achieved by using a setup that measures purely one handedness and run a complete spectrum, then measure another spectrum for the other handedness. Figure 3.4 shows a block diagram of the modular CPL spectrometer. Laser excitation of the Eu^{3+} and Tb^{3+} complexes was accomplished using a Elforlight UVFQ series diode pumped solid state Nd:YAG laser operating at the third harmonic (355 nm). The maximum average power rating of the laser was 400 mW, with maximum pulse energy of 200 µJ. The pulse frequency range was 5 kHz. The collimating lens collects the emission from the sample holder aperture, in a 1 cm quartz cuvette and focuses it to infinity along the primary optical axis of the instrument. The light excites the sample and the emitted light is collected perpendicular to the incident light. The emitted light is then passed through the PEM, which operates as a 50 kHz photoelastic quarter-wave modulator, which together with a linear polariser acts as a circular analyzer. The orientation of the quarter wave plate must be such that the plane is at 45° relative to the plane of polarisation of the incoming light otherwise, the resulting light will be elliptically polarised. The light is focused into a monochromator which scans a selected wavelength range (520-720 nm Eu) before passing through the PMT. The 50 kHz modulation in the emission beam corresponds to alternately left then right CP detected light. The input and output slits of the MC (Princeton Instruments Acton 2155) were both set at 0.25 mm width, corresponding to a spectral resolution of 0.5 nm. The emitted radiation is then detected by the PMT and its wavelength determined by the emission MC. The PMT used was based on a Hamamatsu H10723 series photomultiplier tube module, wired to a control box. To extract, $\Delta I(\lambda)$, the signal from the PMT must be passed through a LIA which reduces noise signal and produces an output AC and DC signal. The LIA (Hinds instrument) matches the PEM phase polarisation modulation to the PL difference acquisition which is subsequently converted to a digital format which can be manipulated analysed by

the PC. A positive phase represents left-handed circular polarisation, while the negative phase represents right-hand circular polarisation. The AC output of the phase sensitive detector is proportional to the CPL intensity. The DC signal is the sum of the total intensity. The two values are used to calculate the g_{em} factor in equation 2.8 and 2.9. From the experiment we therefore obtain the CPL through the AC and DC signals as,

$$g_{em} = \frac{2 \times AC}{DC} \qquad \text{(Eq 3.1)}$$

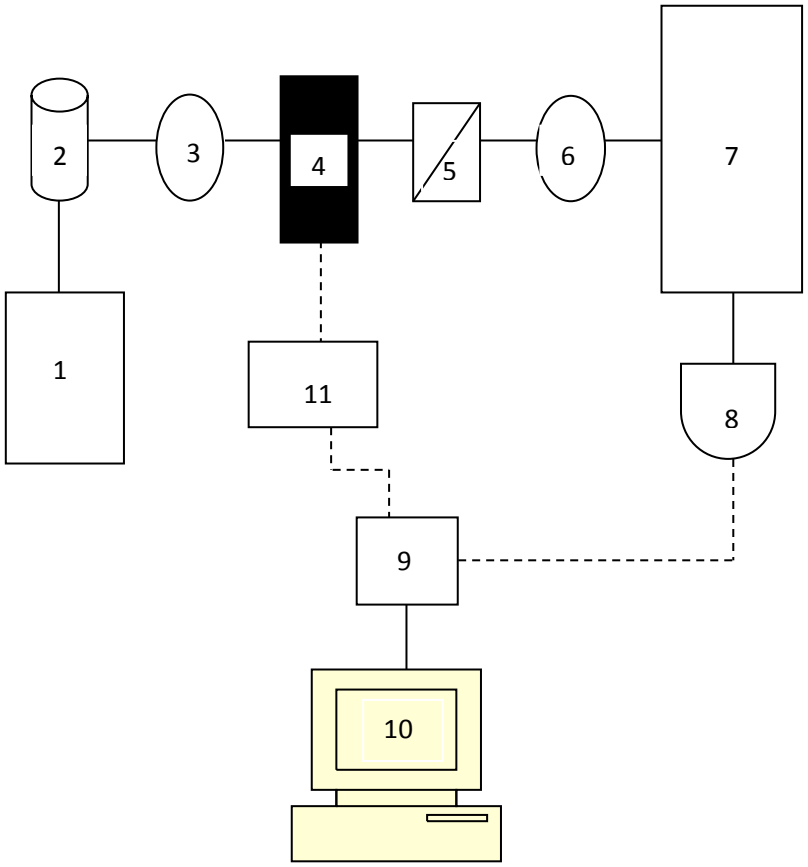

Figure 3.1: Basic block diagram of the Durham CPL spectrometer. (1) Excitation source, (2) Sample holder, (3) Collimating lens, (4) PEM, (5) Polariser, (6) Lens, (7) Monochromator, (8) PMT Tube, (9) Lock-in amplifier, (10) PC , (11) PEM control. The dash lines represent electronic connections and the normal line represents emission pathway.

3.2 The Components of the Modular CPL Spectrometer.

3.2.1 Excitation Source.

The Nd:YAG) laser is a crystal used as a lasing medium for solid-state lasers. The Neodymium ion provides the lasing activity in the crystal. The maximum pulse frequency was used, in order to maximise total luminescence. As the laser light is being passed through five metres of fibre optic cable, any polarisation inherent in the light source is very effectively destroyed.

3.2.2 Sample Holder.

The sample holder is designed to hold a 1 cm cuvette such that when filled with 1 cm^3 of liquid, the maximum possible volume of sample can be excited without excitation light reflecting or refracting off the edges of the cuvette or the sample-air interface, and the maximum possible amount of light can be collected by the collimating lens. The sample holder is also equipped with a mirror on the back side which will reflect the emission light travelling in the opposite direction relative to the detection system. This enhances the sensitivity of the experiment. The excitation emission geometry is in a perpendicular configuration as can be seen in figure 3.1. This will ensure that no stray excitation light will interfere with the PL from the sample material.

3.2.3 Lens and Optics.

The lens assembly is a collimating lens, which collects the emission from the sample holder aperture and focuses it to infinity along the primary optical axis of the instrument. This reduces the incident angle of the emitted light on the PEM head to near zero, maximising its effectiveness as a phase retarder. The lens focuses the light onto the diffraction grating in the MC. Another lens focuses the light from the MC onto the PMT detector. The optics used for this spectrometer have an anti-reflective coating (a Comar Optics PB/VB range coating, giving ~0.5% reflectance over the 450-900 nm range), which is suitable for the 470-720 nm range used for the detection of the Ln^{3+} PL.

3.2.4 PEM and Linear Polariser

A Hinds PEM-90 head was used in this setup. A PEM is an optical device which modulates the polarisation of a beam of light by making use of the photoelastic effect. The principle of operation is based on the photoelasticity in which a mechanically stressed sample exhibits birefringence proportional to the resulting strain. The PEM-90 consists of a rectangular bar of a suitable transparent solid material (fused silica) attached to a piezoelectric transducer. If the transparent solid material is stressed by compression or stretching, the material becomes birefringent meaning that different linear polarisations of light have slightly different speeds of light when passing through the material. The level of birefringence can be selected by changing the amplitude of the applied voltage. This selectivity allows the PEM to scan across a range of wavelengths without the distortion in the wavelength domain that would be imparted by simply using a quarter wave plate. The fact that the PEM scans means that the photon detection system used has to be a combination of a scanning MC and a PMT, instead of a CCD, otherwise the aforementioned distortions in the wavelength domain would kick in. The CP to LP function of this device can be tuned for maximal efficiency at different wavelengths, combating the fact that quarter wave plates are only effective across a narrow range. To extract the polarisation difference signal, denoted $\Delta I(\lambda)$, the signal from the detector must be passed through a lock-in amplifier; LIA.

3.2.4.1 Retardation Effects

The plane of polarisation is at 45° to the modulator axis before passing through the modulator. The effect of the modulator on a linear polarised monochromatic light is that if the optical element is relaxed, the light passes through with the polarization unchanged. If the optical element is compressed, the polarisation component parallel to the modulator axis travels slightly faster than the vertical component after light passes through the modulator. If the optical element is stretched the horizontal component lags behind the vertical component. The phase difference between the components at any instant of time is called the retardation.

3.2.4.2 Quarter Wave Retardation.

When the peak retardation reaches ¼ th of the wavelength of light the PEM acts as a quarter wave plate. When the modulator retardation reaches +λ/4, the right handed CPL is produced and at –λ/4, left handed CPL is produced. This is illustrated in Figure 3.3.

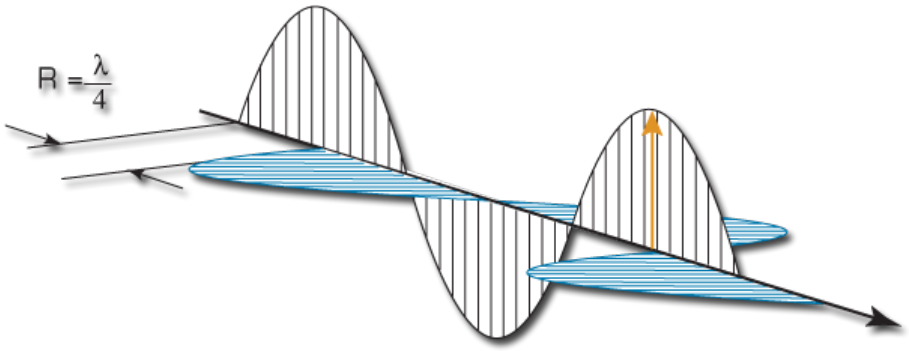

Fig 3.2: Quarter-wave retardation leading to circularly polarised light.

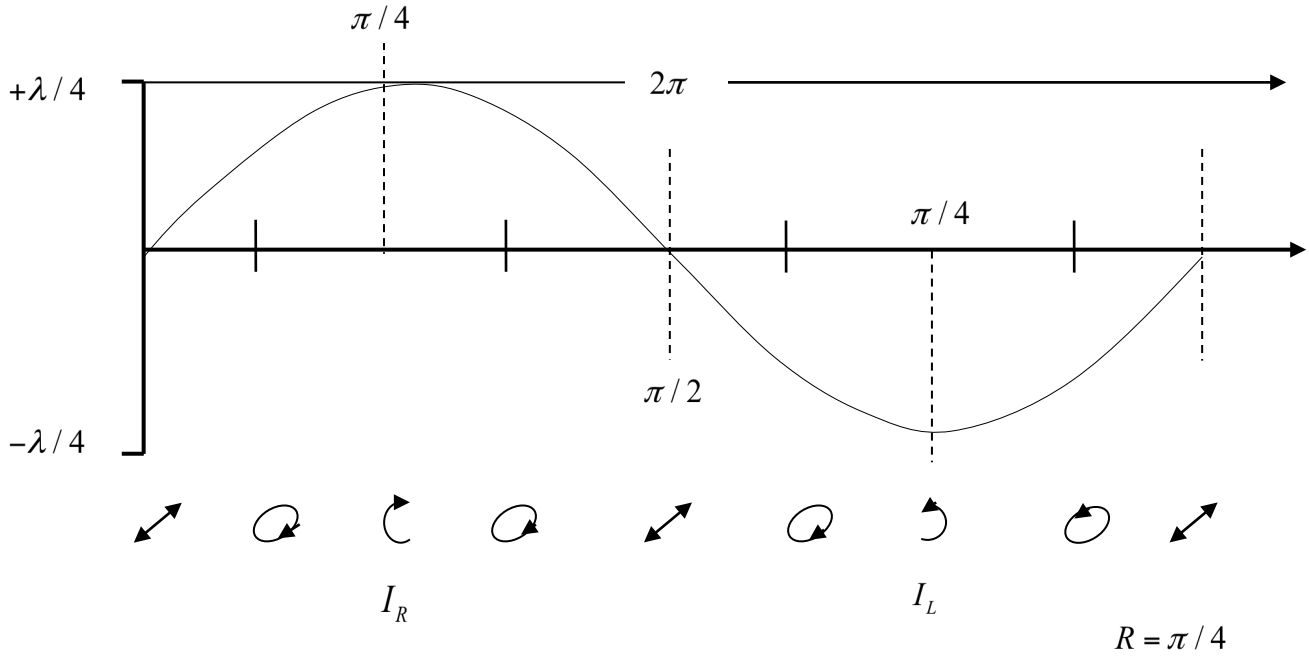

Fig 3.3: Retardation vs time.

Hence, the quarter wave plate is used to convert CP light to LP light. The two handednesses being converted into LP light in two orthogonal planes. With an LP filter after the quarter wave plate set to pass one plane, the other plane is eliminated.[1] Rotating either component by 90 degrees changes the handedness of CP light passed. Although this approach works, it can sometimes be flawed by fluctuating temperature, which alters the sensitivity of the detector or PL of the sample. A much better way to approach the measurement is to build a system, which can rapidly and accurately switch between the two discriminatory states.

3.2.5 Monochromator

The monochromator is an optical device that transmits a mechanically selectable narrow band of wavelengths of light or other radiation chosen from a wider range of wavelength. It consists of a dispersive element, an entrance slit and mirrors to create a parallel beam similar to sunlight, and an exit slit and mirrors to extract the monochromatic light. Light containing various wavelengths can be broken down according to the wavelength. White light entering the monochromator is extracted as green (540 nm), red (650 nm), or some other monochromatic single-wavelength light. The operating principle can be explained by an experiment using a prism to break down sunlight, as shown in Figure. 3.4. A slit can be inserted in the rainbow to extract monochromatic light. Fixing the slit and rotating the prism rotates the direction of the rainbow such that the colour of the extracted monochromatic light changes.

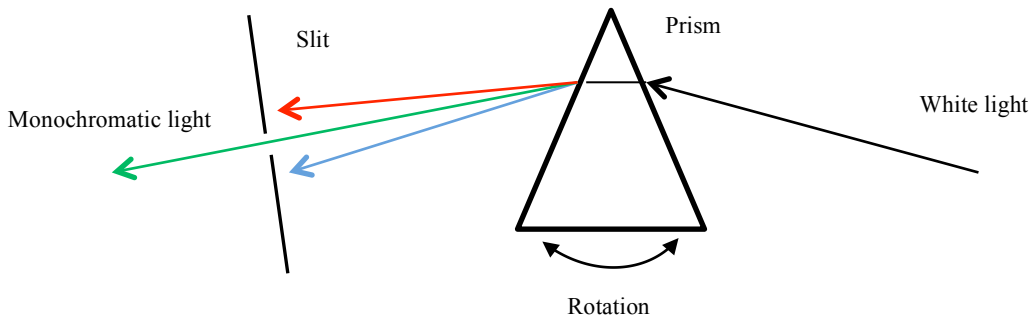

Fig 3.4: Monochromator with prism set-up

Breaking down light into its constituent wavelengths similar to a rainbow is known as dispersion. An element with this property is called a dispersive element. The prism is a typical dispersive element. Another dispersing element is the diffraction grating, which was the setup used for this project. Laser light shining onto a diffraction grating through an entrance slit reflects back in rainbow colours in the same way as a prism, the diffraction grating can be rotated to change the colour of the light extracted through the slit. The slit makes sure that the incoming light beams are parallel and that there is no stray light. The light is then reflected off two mirrors and directed onto the diffraction grating. The diffraction grating has a jagged edge and takes the incoming parallel light beams and makes them non-parallel. Due to the grating being at a non-perpendicular angle to the incoming light, the light is reflected off the gratings at different angles depending on the wavelength. The deflected light hits final mirrors that separate the light beams even further. A certain wavelength is set for the experiment and the grating turret moves so that the desired wavelength of light will be directed out of the exit slit and onto the sample as illustrated in Figure 3.5.

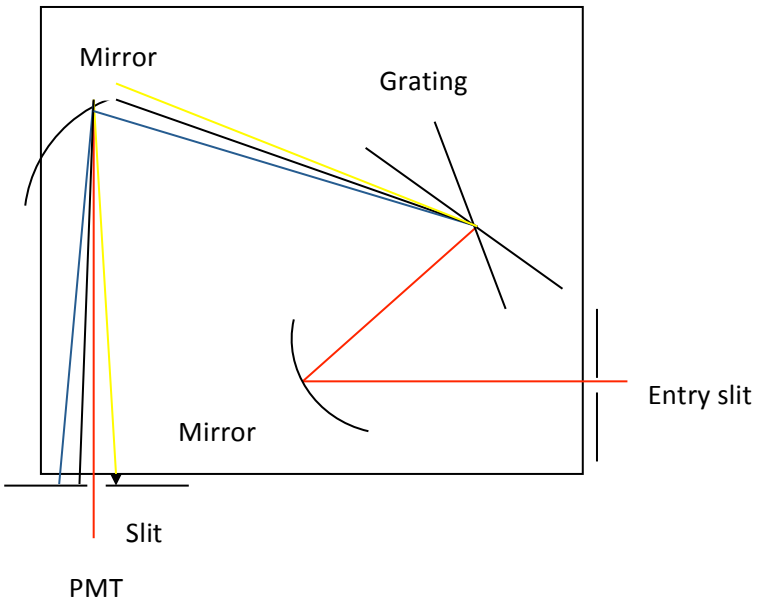

Fig.3.5: Using a Diffraction Grating.

The slits of the monochromator will narrow down the spread light pathways entering and exiting the monochromator (prism or grating based system). As a consequence

the resolution of the transmitted light is narrower and well defined (with narrow slits). However, the drawback is that this limits the intensity and it is therefore necessary to find a suitable trade-off between resolution and signal intensity.

3.2.6 PMT

PMT is a vacuum tube consisting of an input window, a photocathode, focusing electrode, an electron multiplier and an anode usually sealed into an evacuated glass tube. The incident light which enters the PMT is detected and produces an output signal through the following process; light passes through the input window; the light then excites the electrons in the photocathode so the photoelectrons are emitted into the vacuum. Photoelectrons are then accelerated and focused by the focusing electrode onto the first dynode where they are multiplied by means of secondary electron emission. The secondary emission is repeated at each successive dynode. The multiplied secondary electrons emitted from the last dynode are then finally collected by the anode.

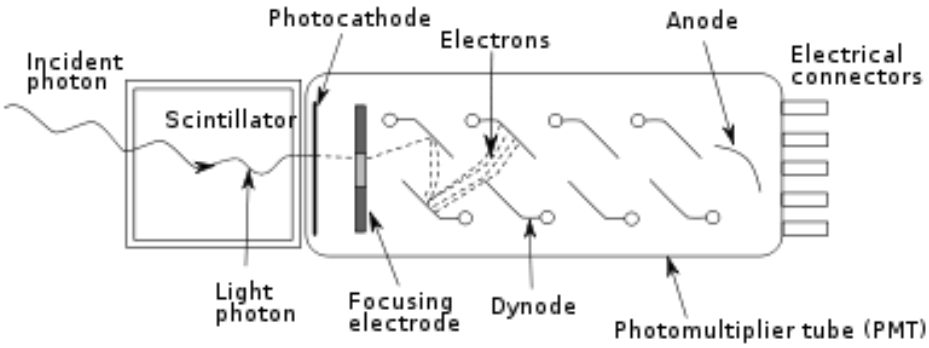

Fig 3.6: PMT showing the photocathode, dynodes and anode

The PMT used was a homebuilt model centred around a Hamamatsu H10723 series photosensor module, wired to a control box provided by the electronic workshop, with adjustable gain.

3.2.7 Lock In Amplifier - LIA

The LIA collects the electronic signal from the PMT and converts it into a CPL signal. This is achieved using the technique known as phase sensitive detection. This a

method for seeing small signals in the presence of overwhelming noise. The lock-in effectively responds to signals, which have the same phase and frequency as a reference waveform. The reference is this case is the PEM operating frequency. By locking the phase of the lock-in (hence the name) to this frequency, measurements can be made of the PMT signal at points in the PEM cycle corresponding to the passing of certain polarisation states of light. The lock-in calculates the difference between the signals. If there was no CP emission, this would clearly be zero. Predominantly left-handed CP emission would give a positive signal, and right-handed CP emission vice-versa. This AC signal extracted is thus equal to $\Delta I(\lambda)$ (assuming the various filters are in the correct orientation and the instrument has the correct phase factor). The DC signal, which is the sum of $I_L(\lambda)$ and $I_R(\lambda)$, is equal to the total emitted intensity, $I(\lambda)$. These two signals are the output signals of the LIA and directly proportional to total emission and the CPL given by the difference signal $\Delta I(\lambda)$. The LIA thus produces signal intensities that are measured (and plotted) in units of millievolts (mV). These two values can then be used to calculate the emission dissymmetry factor, g_{em}. The lock-in also eliminates noise[1]. It does this by only sampling the PMT output at the frequency of the PEM - any frequencies outside the narrow window the lock-in allows are discounted. This includes all of the low frequency noise from (but not limited to); mains hum at 50 Hz (and higher harmonics), variations in the dark current of the PMT, variations in background light that will inevitably leak in to the system, and so on.

The model used here is a Hinds Instruments Signaloc Model 2100, which is tailored for use with Hinds Instruments PEM. This model has a frequency response of 40 Hz - 250 kHz with the PEM operating at 42 kHz. Instrumental noise scales as 2μV/$\sqrt{Hz}$, or ~0.4 mV at operating frequency. Gain accuracy is ±1% of maximum for signals ≥1 mV (the majority of signals), and ±5% for weaker signals.

3.3 Validation of the CPL Spectrometer.

The operation of the spectrometer was tested and calibrated using a red, green and blue LED light as the light source, which gave the same results. The unpolarised emission of the LED was passed through a linearly polarising filter and the quarter wave plate. Two spectra were measured, with the discriminating polariser rotated by

ninety degrees. This produced a mirror image differential spectrum, confirming that the instrument was capable of discriminating between polarisation states of LP light. To test the instrument for CP light, the sample and quarter wave plate pairing later used for instrument calibration was measured. To test how effective the spectrometer was, a CPL spectrum was taken of the emission of a red LED passed through a quarter wave plate. The CPL signal is ~90% of the total intensity, corresponding to a g_{em} value of +1.8 (the theoretical maximum is 2 as dictated by equations 2.9 and 2.10). This gives an underestimation of 10%. Given that the quarter wave plate is not a perfect converter of LP-to-CP light, due to its broad band range, this figure is likely closer to ~5%. This result is shown in Figure 3.7

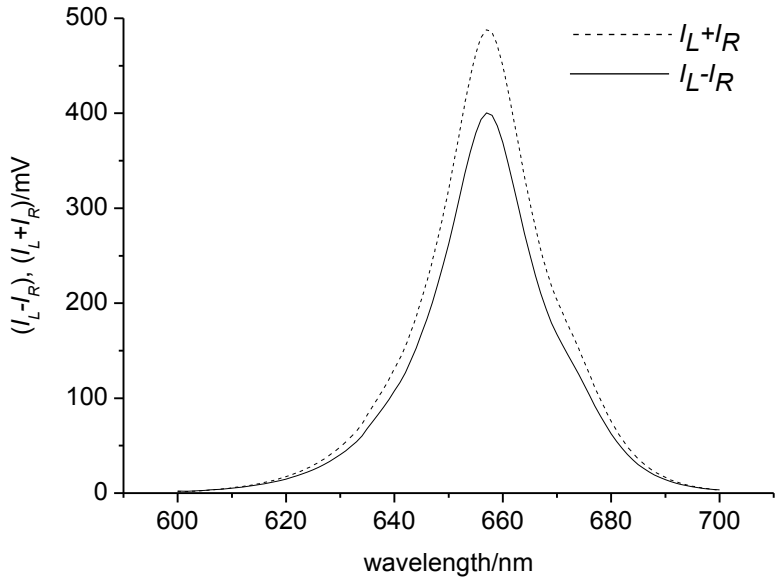

Figure 3.7: Graph showing the efficiency of the spectrometer. The total signal *I* is the dashed line, ΔI is the solid line. Reproduced from Carr et al[2].

3.4 References.

1. J. P. Riehl and G. Muller, Circularly polarised luminescence spectroscopy and emission-detected circular dichroism, Wiley, New Jersey, 1st edn., 2011.
2. R. Carr, R. Puckrin, B. K. McMahon, R. Pal, D. Parker and L.-O. Pålsson, Induced circularly polarized luminescence arising from anion or protein binding to racemic emissive lanthanide complexes. *Methods Appl. Fluoresc.*, 2014, **2**, 024007.

4 CPL SPECTROSCOPY OF dpqC SAMPLES (Eu^{3+} and Tb^{3+} COMPLEXES).

4.1 Introduction.

The Ln^{3+} complexes used for this work possess the tetramacrocycle ligands (fig 4.1) based on DOTA ring structure. They are a significant group of Ln^{3+} complexes and a large family of water soluble ligands based on the 1,4,7,10-tetraazacyclododecane skeleton (cyclen) as the core ligand element. Functionalised with donor groups such as carboxylate (DOTA), phosphinate, amide or amino acid 'arms' (e.g DOTAM) to the N of the cyclen ring to make up a hexa or hepta dentate moiety to shield the ion very effectively, these ligands form a cage like ligand and display extremely stable kinetic and thermodynamic properties. Depending on the charge of the donor groups, the resulting complexes may be cationic, neutral, or anionic. Fig. 4.1 shows a typical tetrazamacrocycle, dpqC, in which either Tb^{3+} or Eu^{3+} is bound.

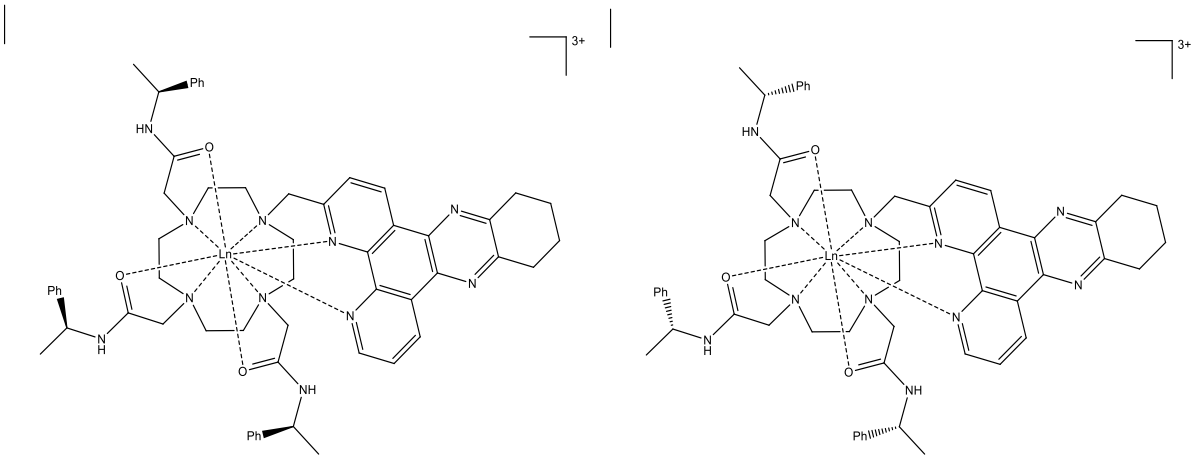

Figure 4.1 Right structure: *SSS*-Ln^{3+} $(PhMe)_3$(dpqC). Left Structure: *RRR*-$Ln^{3+}(PhMe)_3$(dpqC). Ln^{3+} (Eu^{3+} or Tb^{3+})

The sensitiser used in this study is the tetraazatriphenylenes (dpqC). It is a judiciously selected aromatic or heterocyclic moiety. Figure 4.2 shows the dpqC chromophores and its photophysical properties outlined below as revealed through a series of PL Eu^{3+} and Tb^{3+} complexes.

Ln^{3+} complexes with dpqC were first reported in 2003 by the Parker group at Durham.[1] This family of organic chromophores not only acts as an efficient sensitiser for Eu^{3+} and Tb^{3+} complexes, but may also intercalate between the base pairs of

DNA. [1] The complexes have an absorbance maximum at 340 and 350 nm and emit with a millisecond lifetime in the range 480 to 720 nm. Such features avoid problems associated with autofluorescence and Rayleigh scattering. Each complex also possesses a high overall quantum yield (Eu^{3+} = 0.16, Tb^{3+} = 0.40 in water, 295 K) [2.] The triplet energy is around 24000 cm^{-1} (the singlet around 29000 cm^{-1}) [2], which is ideal for transferring energy to the Tb^{3+} and Eu^{3+} excited states at 17420 cm^{-1} and 20400 cm^{-1}.

The side arms of the tetramacrocylces are functionalised with donor groups, in this case, phenylalanine, to shield the Ln^{3+} ion very effectively. Upon pendant arm ligation, enhanced shielding from intermolecular ligation of chelating species, or quenching effects of the solvent water molecules may be achieved, resulting in increased metal based luminescence. [3] The Ln^{3+} complex also contains a chelate which serves several purposes, including binding the Ln^{3+} tightly, shielding the Ln^{3+} ion from the quenching effects of water, and acting as a scaffold for attachment of the antenna and a reactive group (either amine or thiol) and the latter for coupling the chelate complex to biomolecules.

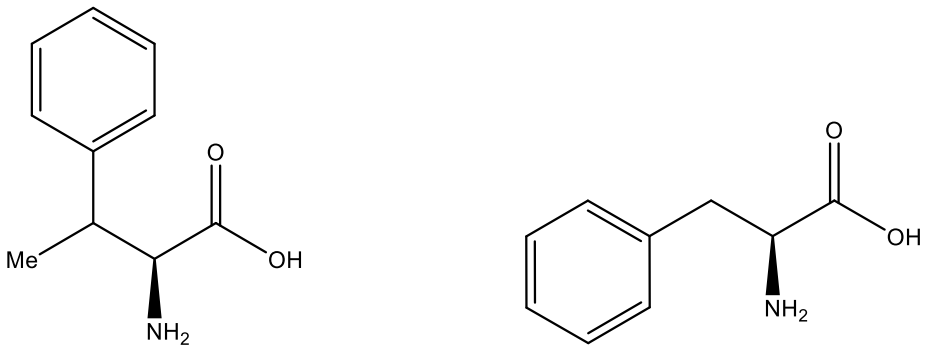

Figure 4.3 Right: *S* phenylalanine side arm. Left: *R* phenylalanine side arm.

4.2 Materials.

R.S.Dickins *et al* [4] reported the synthetic procedure for these compounds used for the preparation of the complexes.

4.3 Results and Discussion.

As expected, the total PL spectra for the two enantiomers of Tb^{3+} complexes are identical in structure, but show small differences in intensity. Hence, PLQY are similar (care was taken to normalise the linear absorption to ~0.3 for all sample materials). The ΔJ = 1 band is the most prominent peak. As can be seen in figure 4.5, differences in helicity have no impact on the structure of the total emission, spectrum but can be easily observed in the CPL spectra of the two enantiomers, which are mirror images of each other, i.e the *RRR* enantiomer of Tb^{3+} exhibits almost the exact mirror image spectrum to the *SSS* enantiomer with respect to line shapes as well as intensity. The ΔJ = 1 is strong in CPL as expected as this is the MD transition.

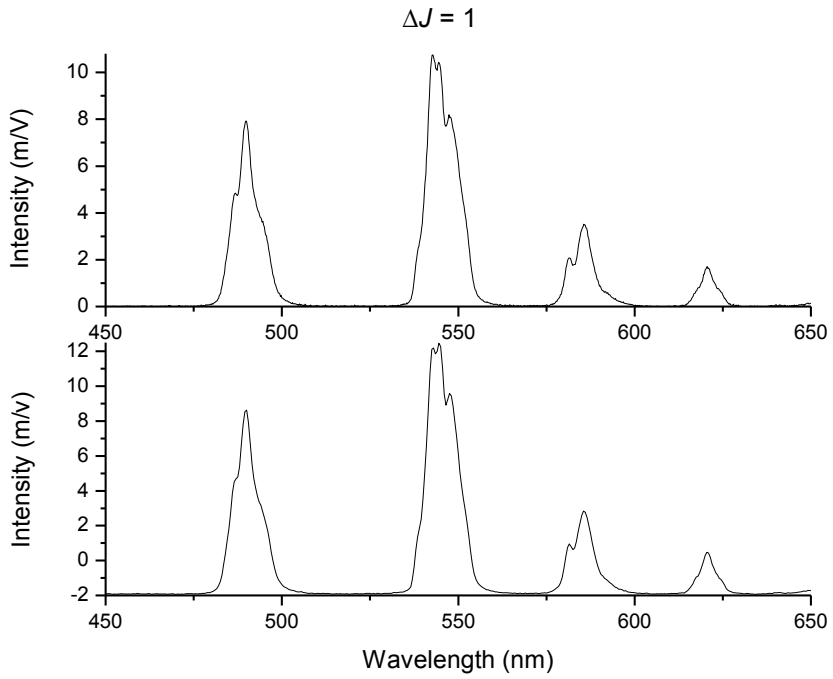

Figure 4.5: Top: Emission spectra of *SSS*-Δ-Tb(PhMe)$_3$(dpqC). Bottom: Emission spectra of *RRR*-Λ-Tb(PhMe)$_3$(dpqC)

It can also be observed in both the PL and CPL spectra that there is a splitting into 3 sub-bands of the ΔJ = 1 band. This is indicative of a crystal field effect causing splitting due to different environments. The CPL spectra clearly show this splitting as the CPL in the ΔJ = 1 region splits into three different bands. That the CPL is more

sensitive to these types of effects has been discussed previously by Richardson et al.[4]

Figure 4.6 shows the CPL spectra of the two enantiomers normalised to the total emission seen in figure 4.5. As can be seen they display near to perfect mirror image spectra. This is due to opposite helicities around the metal centre for the two Ln^{3+} complexes. However, these are not stable and this thus leads to racemisation, which in turn results in a loss of CPL due to cancellation polarisations. An example is the ring conversion, which occurs at room temperature at a rate of 50 – 100 Hz, as previously mentioned.

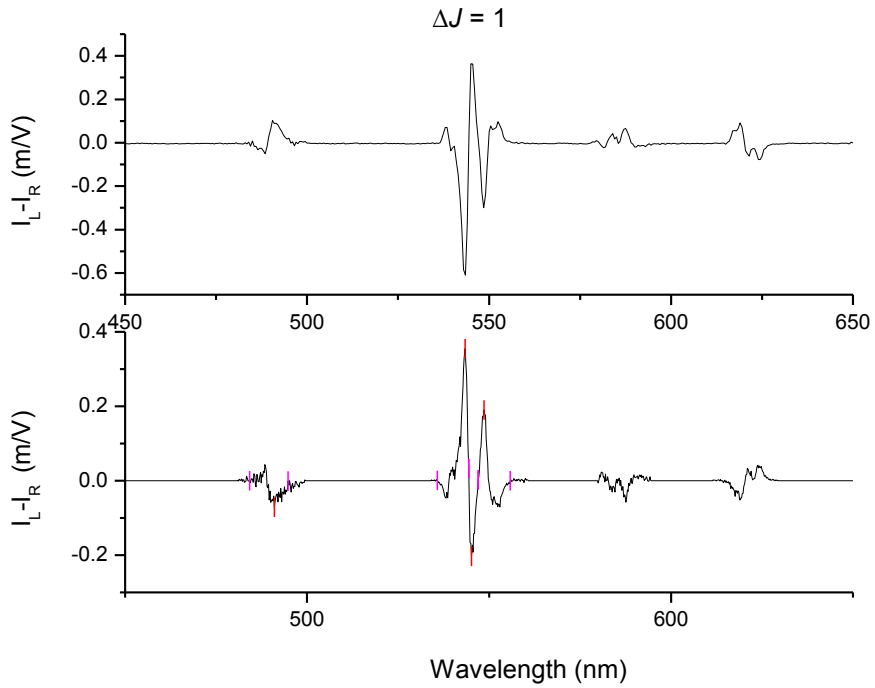

Figure 4.6: Top: CPL spectra of (RRR)-Λ-Tb(PhMe)3(dpqC). Bottom: CPL spectra of *SSS*-Δ-Tb(PhMe)3(dpqC)

The Ln^{3+} complexes used here are structurally modified to prevent racemisation, which in turn results in a well-defined CPL.[5] The modification is the Phenyl functional group attached the side (pendant) arms of the Ln^{3+} complexes which is introduced with different chiralities. The effect this has is that the Ln^{3+} complexes are locked into a specific conformation thus preventing racemisation due to steric hindrance. This results in well-defined CPL, which is controlled through the chirality of the Phe functional group.

For the Eu^{3+} complex, only the *SSS* isomer was available for analysis. For the total emission spectra, the strongest emission are from the ΔJ = 1 and ΔJ = 2. The ΔJ = 1, which is MD in character is largely independent of the coordination sphere whereas the ΔJ =2, electric dipole is extremely sensitive to the coordination sphere and the symmetry around the ions as well as presence of polarisable groups. ΔJ = 0 is weak, but can be sensitive to the ligand environment. The ΔJ = 3 transitions is extremely weak while ΔJ = 4 is also sensitive to the polarisability of the donor ligands atoms. By contrast; in the CPL spectra, ΔJ = 1 and ΔJ = 3 are strong compared to ΔJ = 2, which has small intensity as both the former transitions have MD character.

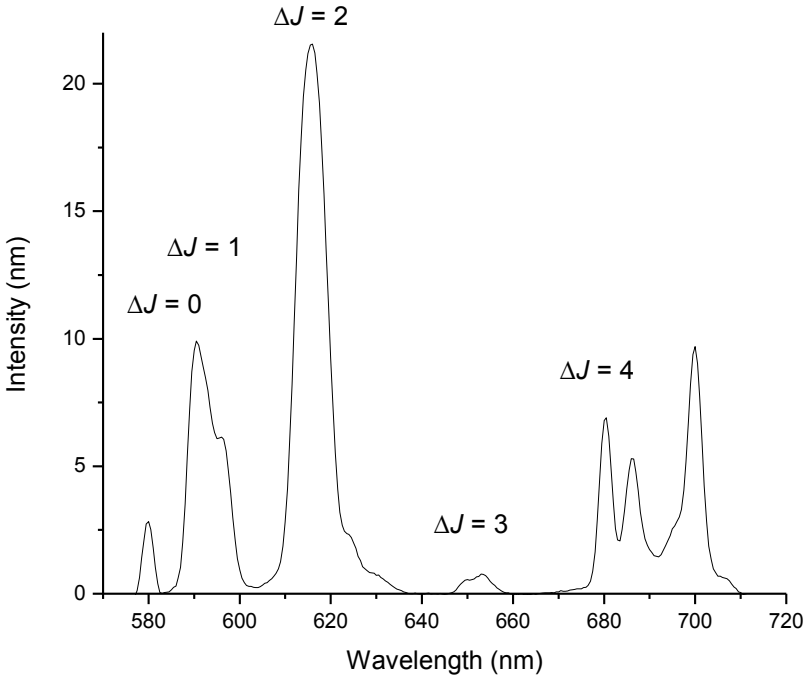

Figure 4.7: Emission spectra of SSS-Δ-$Eu(PhMe)_3(dpqC)$

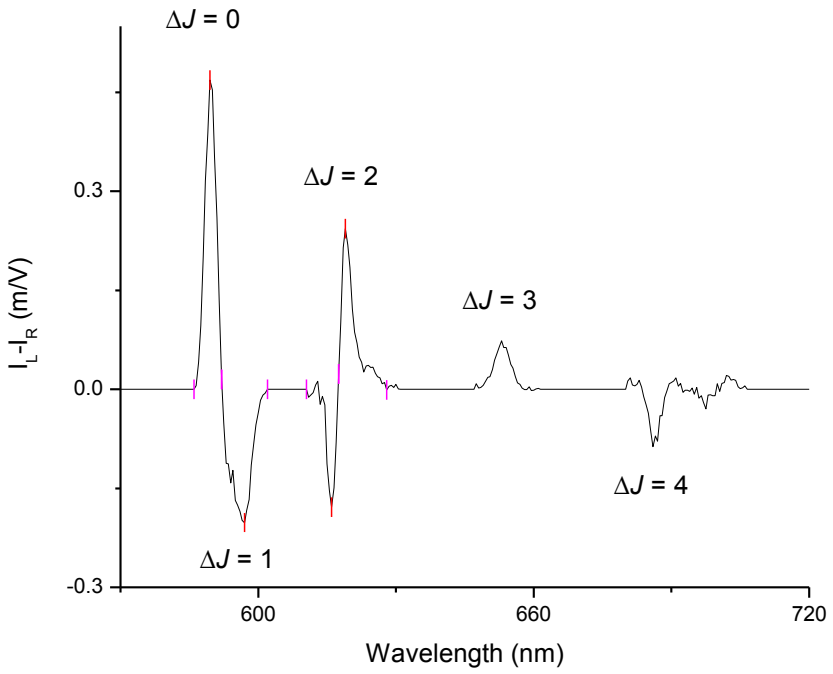

Figure 4.8: CPL spectra of *SSS*-Δ-Eu(PhMe)$_3$(dpqC)

The g_{em} values have been calculated using equation 2.7, and are shown in tables 4.1 and 4.2. The g_{em} values for the two enantiomers of Tb^{3+} at each wavelength are almost identical in magnitude but with opposite sign except ΔJ = 1 and ΔJ = 2 as the magnitude is slightly higher in the *RRR* isomer compared to the *SSS* isomer. However, the data in table 4.1 essentially confirms the mirror image properties of the CPL that was evident in the spectra of the enantiomers.

Transition (ΔJ=)	Wavelength (nm)	(*SSS*) isomer	(*RRR*) isomer
0	491	-0.029	0.027
1	545	-0.045	0.068
2	590	0.011	-0.046
3	620	-0.033	0.032

Table 4.1: Table showing the g_{em} values of the transitions in the Tb^{3+} based dpqC complexes.

Transition (ΔJ=)	Wavelength (nm)	(*SSS*) Eu(PhMe)$_3$(dpqC)
0	580	-0.007
1	590	0.127
2	613	-0.001
3	650	0.053
4	690	-0.017

Table 4.2 Table showing the g_{em} values of the transitions in the Eu^{3+} based dpqC complexes.

4.4 Conclusion.

Previous work done by Montgomery *et al.* [6] showed that interaction of the *SSS*-Δ enantiomer of Tb^{3+} and Eu^{3+} complex with proteins will induce inversion of the helicity on the CPL. Montgomery studied a chiral optical probe for albumin where reversible protein binding was signalled by a switch in the CPL associated with helicity inversion (Δ to Λ) of the enantiopure Ln^{3+} complex. Selective binding of dynamically racemic Ln^{3+} complex to proteins can lead to a significant change in the Ln^{3+} total emission spectra as well as switching on CPL signal from the metal centre. Ln^{3+} complexes can interact with proteins in two ways; first at the metal centre where a protein residue displaces a solvent and secondly, through a non-covalent binding interaction between the sensitizing moiety and a protein binding pocket.

These results show how powerful the methodology is to probe these stereo specific interactions for future work. The CPL spectroscopy will therefore set the scene for developing CPL microscopy based on functionalised chiral Ln^{3+} complexes. Monitoring a judiciously chosen CPL transitions in CPL microscopy will facilitate a method to probe the content and distribution of chiral species in cells. The net sign of the bands will be monitored by examining the effect on CPL as a result of interaction between the Ln^{3+} complex and chiral species in cells.

Band pass detection using narrow band pass filters will be used to monitor the MD transition, ΔJ = 1 of Eu^{3+} and Tb^{3+} complexes as these are strongest most intense transitions. The Leica microscope allows spectral imaging using the internal

scanning system. However for the CPL detection, it is not feasible to use the spectral imaging capability, as the resolution would not be sufficient for this purpose.

4.5 References.

1. J. C. Frias, G. Bobba, M. J. Cann, C. J. Hutchison and D. Parker, *Luminescent nonacoordinate cationic lanthanide complexes as potential cellular imaging and reactive probes. Org. Biomol.Chem*., 2003, 1, 905-907.
2. E. J. New, D. Parker and R. D. Peacock, *Comparative study of the constitution and chiroptical properties of emissive terbium and europium complexes with a common tetraazatriphenylene sensitiser; the nature of the sensitiser determines quenching sensitivity and cellular uptake*, Dalton Trans., 2009, 4, 672–679.
3. D. Parker, R. S. Dickins, H. Puschmann, C. Crossland, and J. A. K. Howard, *Being Excited by Lanthanide Coordination Complexes: Aqua Species,Chirality, Excited-State Chemistry, and Exchange Dynamics* Chemical Reviews., 2002, 6, 1977-2010.
4. R. S. Dickins, J. A. K. Howard, C. L. Maupin, J. M. Moloney, D. Parker, J. P. Riehl, G. Siligardi and J. A. G. Williams, Synthesis, *Time-resolved luminescence, NMR spectroscopy, circular dichroism and circularly polarised luminescence studies of enantiopure macrocyclic lanthanide tetraamide complexes*, Chem. Eur. J., 1999, 5, 1095-1105.
5. S. Pandya, J. Yu and D. Parker, *Engineering emissive europium and terbium complexes for molecular imaging and sensing;* Dalton Trans., 2006, 23, 2757-2766.
6. C. P. Montgomery, E. J. New, R. D. Peacock and D. Parker, Enantio selective regulation of a metal complex in reversible binding to serum albumin: dynamic helicity inversion signalled by circularly polarised luminescence. *Chem.commun*., 2008, 36, 4261-4263.

5 ANION INDUCED CPL SPECTROSCOPY OF THE 9N3 MACROCYCLE (Eu^{3+}).

5.1 Introduction.

Reversible anion binding at Ln^{3+} centres in aqueous media has emerged as an effective means of signalling and sensing the presence of selected anions[1]. There are three distinct behaviours that can be observed and distinguished following anion binding. The first involves reversible binding of the anion to the Ln^{3+} centre with displacement of coordinated water or a weakly bound ligand donor. Anion binding in this case can switch on Ln^{3+} emission, if the anion has a suitable chromophore with a triplet energy lying more than 1500 cm^{-1} above the Ln^{3+} emissive state, ensuring back energy transfer [1] is not competitive as the Ln^{3+} complex has an integral sensiter, anion binding leads to displacement of water, changing emission spectral form as the local ligand field varies. This is best reported by Eu^{3+} emission changes. The absence of degeneracy of the emissive ^5D_o Eu^{3+} excited state simplifies its emission spectral form. The intensity of the MD, ΔJ = 1 transitions is relatively unaffected by any coordination change whereas the ED allowed transition, ΔJ = 2 at 615 nm are strongly perturbed. This leads to differences in the relative intensity of the ΔJ = 1 and ΔJ = 2 emission bands allowing ratiometric analysis.

Secondly, reversible anion binding occurs at the ligand-based anion recognition site, perturbing the chromophore ground state. This is usually uncommon, but can be signalled by examining the excitation spectra. Lastly, the anion can encounter the sensitizer excited state, modulating the observed Ln^{3+} emission. This process is usually signalled by the quenching of the excited state and involves electron transfer, which in turn leads to reduction of emission intensity.

Optical activity can be induced in achiral compounds or in racemic mixtures of chiral compounds by dissolution in an optically active solvent.[2] Optical activity initiated in the achiral solute molecules is usually generated by chiral perturbations upon the solute chromophoric group by the solvent molecules. These perturbations may result firstly in chiral distortion [1] of the nuclear configuration of the solute molecule making it inherently optically active. Secondly, they may induce optical activity in chromophoric transitions of the solute molecule through electrostatic interactions between the solute molecules and the electronic charged distributions

on the inherently achiral chromophoric group of the solute molecule or thirdly a combination of both.

Optical activity observed in racemic mixtures that has been dissolved in an optically active solvent is presumed to arise from differential d (solute) - d (solvent) and l (solute) - d (solvent) interactions (in the case where a dextrorotatory solvent is used), which produce an equilibrium mixture of nonenantiometric solute-solvent pairs. The net chirality generated in the formation of these nonenantiometric solvent pairs can lead to observable optical activity.[3]

Studies have shown the reversible and selective binding of a dynamically racemic Eu^{3+} complex to proteins which is characterised by a significant change in the Eu^{3+} total emission spectral fingerprint and the switching on of a large CPL signal from the metal centre. This observation is also very similar with anions. Anion binding can result into three distinctive behaviours. The first involves reversible binding [3] of the anion to the Ln^{3+} centre with displacement of coordinated water or a weakly bound ligand donor where displacement of a coordinated chromophore is signalled by a large increase in emission intensity of the Eu^{3+} $\Delta J = 2$ band, resulting in a switching on of Eu^{3+} emission. For Eu^{3+}, the intensity of the MD transition is usually unaffected by any coordination change, whereas the $\Delta J = 2$ is strongly perturbed. This causes differences in the relative intensity of the pair of emission bands enabling ratio metric analysis to be used. Secondly, reversible anion binding takes place at the ligand-based anion recognition site perturbing the chromophore ground state. This is not common, but can be signalled by examining excitation spectra or by following intensity changes associated with Ln^{3+} emission. Thirdly, [4] the anion encounters the sensitizer excited state and modulate the observed Ln^{3+} emission. Usually, this process is signalled by quenching of the excited state and involves electron transfer. This process is usually then signalled by the quenching of the excited state and involves electron transfer. Ln^{3+} complexes have been shown to bind to anion leading to a change in the form and relative intensity of the observed Eu^{3+} emission.[5]

In this work, it was decided to study the complex binding to five different anions, examining the associated spectral changes. CPL analysis was carried out in solutions containing the anions D- and L- lactate, citrate, D- and L- malate, phthalate, and bicarbonate. The structure of the cationic Eu^{3+} complex analysed in this chapter

is based on the macrocycle called 9N3 (fig 4.1), substituted with a pendant amino arm. The chromophore is based on the pyridine alkynyl aryl moieties. This thesis reports induced CPL from in the presence of selected anions in aqueous solutions.

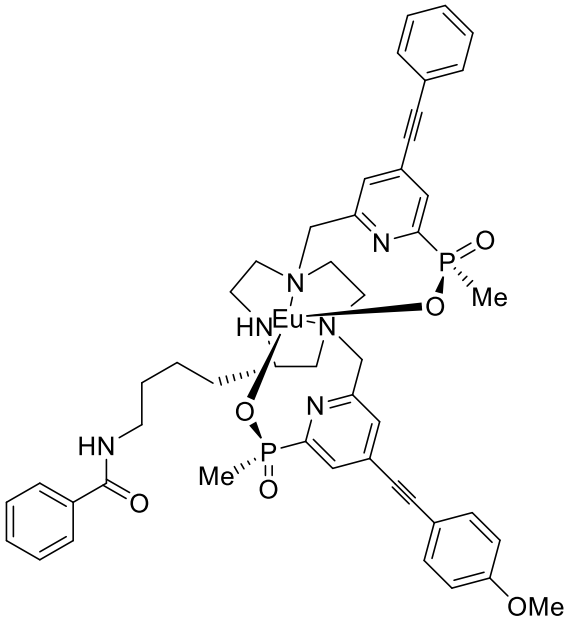

Figure 5.1: Eu^{3+} 9N3 macrocycle substituted with a pendant amino arm.

5.2 Materials.

The functionalised Ln^{3+} complex Eu^{3+} 9N3 was synthesised in Durham by the Parker group (to be published).

Citrate, carbonate, malate, phthalate and lactate were obtained from Sigma Aldrich and used without any further purification and dissolved in high purity water. Ln^{3+} complexes were dissolved in high purity water to a concentration of 0.3M. Anions were added to the solution in excess, typically in concentrations of 10^{-3} M.

5.3 Results and Discussion.

5.3.1 The Eu^{3+} 9N3 Complex in the Absence of Anion.

Fig 5.2 to 5.4 shows the CPL and total emission spectra for the aqueous solution of the Eu^{3+} 9N3 complex over the full spectral range 570 to 720nm. Fig 5.2 shows the spectra in the absence of anion. This complex is different to the DOTA ring systems

as it essentially is C_3 symmetry system, or a version thereof. The following transitions $^5D_0 \rightarrow {}^7F_0$ (580 nm) correspond to the ΔJ = 0, the $^5D_0 \rightarrow {}^7F_1$ (590 nm) corresponds to ΔJ = 1, the $^5D_0 \rightarrow {}^7F_2$ (612 nm) correspond to ΔJ = 2 and the $^5D_0 \rightarrow {}^7F_2$ (650 nm) corresponds to ΔJ = 3 is clearly very weak in these systems. CPL and total emission spectra of the complex were observed under the same conditions for each measurement. The CPL is very weak as can be seen in figure 5.3 but with some signatures in the ΔJ = 1 and ΔJ = 2 regions. Emission dissymmetry factors was also measured and calculated according to equation 2.10 and these are presented in table 5.1. The Eu^{3+} 9N3 complex is a racemic complex and therefore not expected to show any sizable CPL in the absence of any chiral agents.

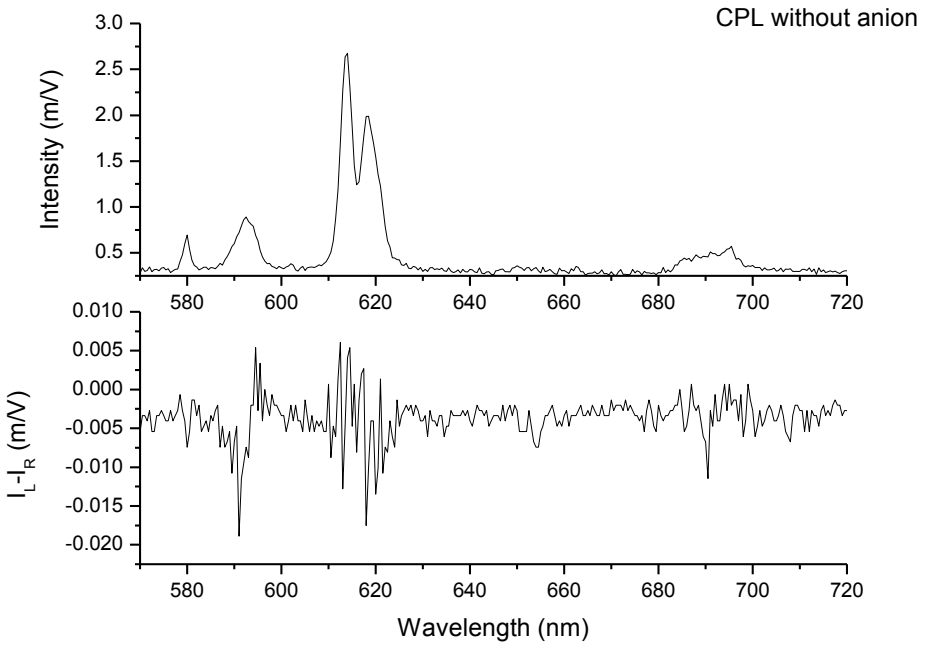

Figure 5.2: Eu^{3+} 9N3 Top: Total emission spectrum. Bottom: CPL spectrum

The total emission spectra shows a split in the ΔJ = 2 region with the ΔJ = 1 transition being slightly asymmetric. This points to different crystal field effects, and therefore slightly inhomogeneous environments. The total emission spectrum is weak and this in turn indicates a low PLQY (not determined in this work). However, a comparison can be made to the total intensity of the SSS-Δ-$Eu(PhMe)^3$(dpqC) seen in figure 4.5 (page 60) which shows ~10 times more intense PL (the experimental conditions are very similar which allows for this comparison).

Transition	Wavelength(nm)	g_{em} factor
$\Delta J = 0$	580	-0.0111
$\Delta J = 1$	590	-0.0108
$\Delta J = 2$	613	-0.0106
$\Delta J = 3$	650	-0.0053
$\Delta J = 4$	690	-0.0130

Table 5.1: Emission dissymmetry factors

The reason for the low intensity, and thus the low PLQT by implication could be due to either one of two factors. Firstly, in the absence of any strongly bound anion water molecules could coordinate to the axial donor on the Eu^{3+} ion which in turn leads to PL quenching due to vibrational energy transfer. The second aspect is that the complex structure may not be as rigid as the DOTA complexes and therefore that structural relaxation could lead to non-radiative decays of the excited state[9]. This would also lead to a low PLQY.

5.3.2 The Eu^{3+} 9N3 Complex in Presence of D- and L- Lactate.

Addition of D/L-lactate results in a substantial increase in PL intensity and thus also the PLQY. Interestingly in the total emission for addition of L- lactate the $\Delta J = 2$ region is now showing more of a homogenous single line shape structure. This would indicate that the environment around it is homogenus.

It could be assumed that the CPL profile of the two enantiomeric forms of lactate would be identical but inverted. However, this was not the case. Although the resultant CPL profiles for the enantiomers were virtually identical the CPL was not inverted as can be seen in figure 5.2. In the presence of added lactate, a change of sign was observed in the $\Delta J = 2$ region, however, the CPL in this region in the absence anions was weak so this observation is somewhat inconclusive. As the g_{em} values for both the CPL in the MD transition for the two enantiomeric forms are near similar, it can be said that the reaction is not stereospecific as the addition of anion in

both lactate forms did not modulate CPL. The splitting observed in the regions of the ΔJ = 1 and ΔJ = 2 emission arise from crystal field induced splitting of the $^7F_1$ and $^7F_2$ free –ion states.

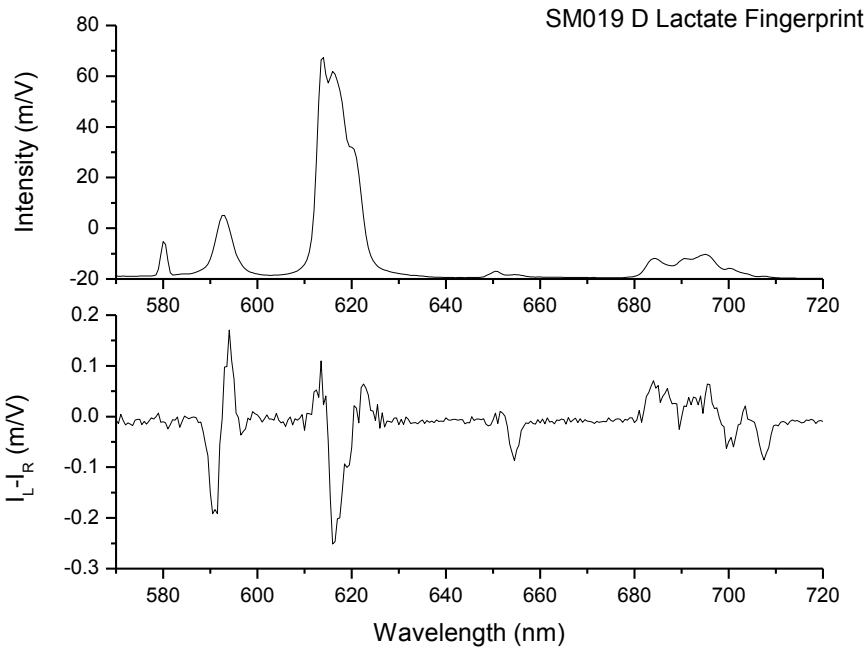

Figure 5.3: D lactate. Top: Total emission spectrum. Bottom: CPL spectrum

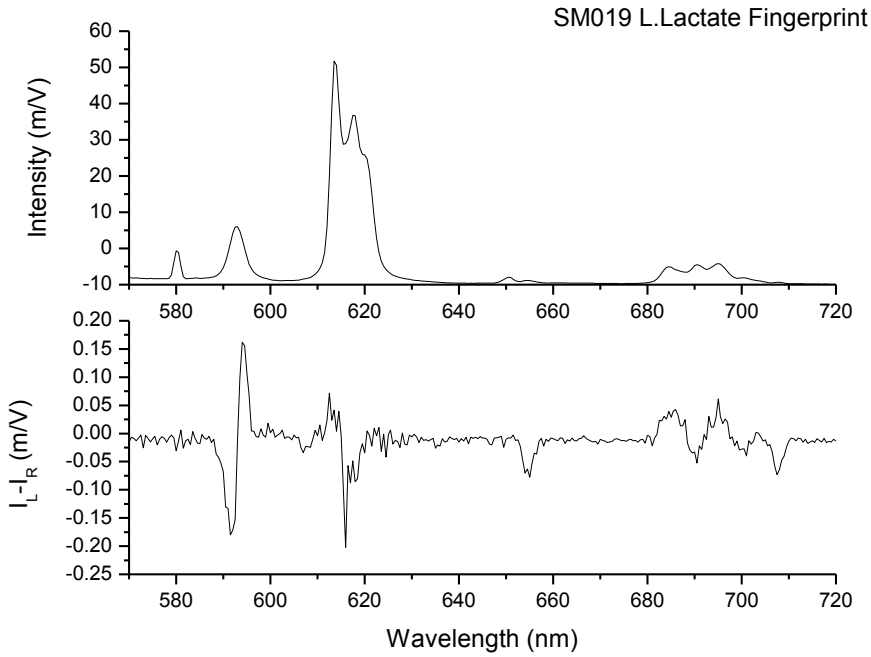

Figure 5.4: L lactate. Top: Total emission spectrum. Bottom: CPL spectrum

There is, however, a clear indication of strong interaction, which is likely to be electrostatic in nature but not stereo-specific, as previously stated. The scenario is therefore that the addition of anion will lead to the replacement of a coordinated water molecule to the axial donor of the Eu^{3+} ion, which in turn leads to a PL enhancement.

Spectra (620 nm)	g_{em} factor
D lactate	
CPL	0.0036
L-lactate	
CPL	0.0032

Table 5.2: g_{em} factor for the MD transition of the total emission and CPL spectra for $\Delta J = 2$

5.3.3 The Eu^{3+} 9N3 Complex in Presence of D- and L- Malate.

The result showed the same pattern for both enantiomers, D- and L- lactate. D-malate appears twice as high as L-malate in the total emission spectra and CPL. Table 4.3 shows g_{em} values. The distinction is, however, that the ΔJ = 2 region now show more of a split for forms of malate. Therefore one can conclude that binding of malate is likely to be stronger although as in the case with lactate, not stereo specificity. This leads to a more rigid Ln^{3+} complex, with less structural relaxation. This in turn leads to a lesser degree of non-radiative decays of the excited state.

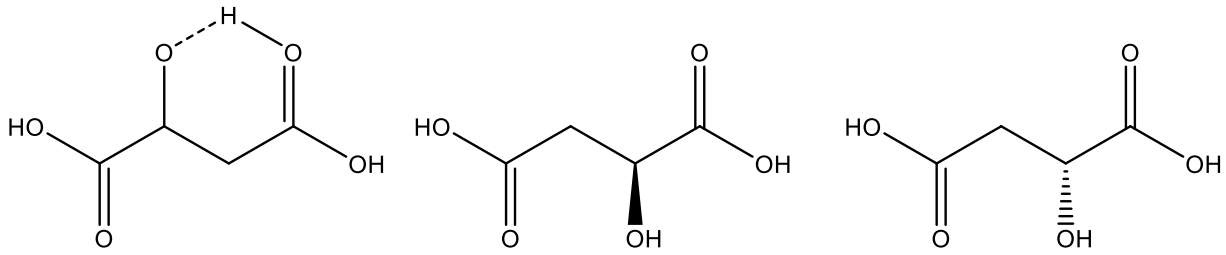

Figure 5.5. The parent acid (left) and the structures of L-malate and (middle) and D-malate (right).

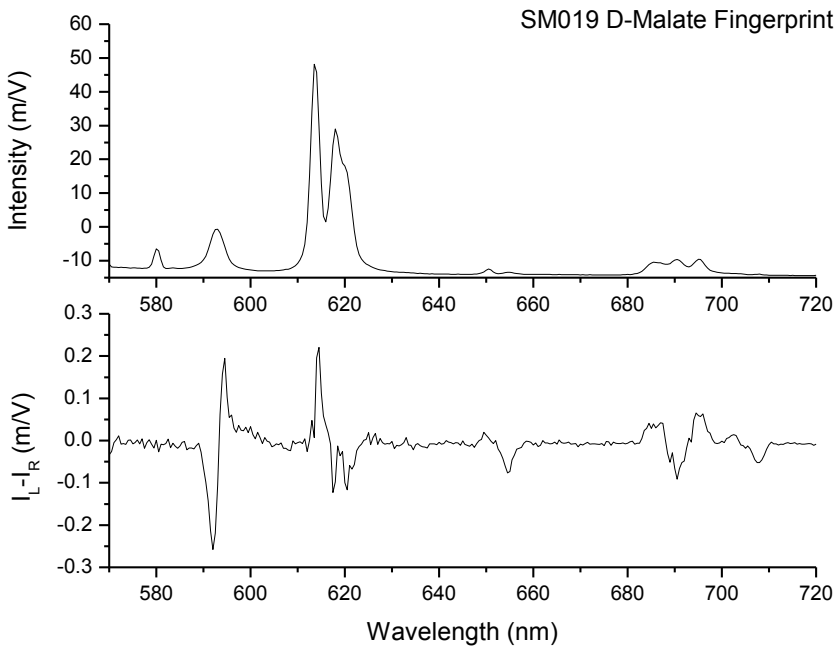

Figure 5.6: D malate Top: Total emission spectrum. Bottom: CPL spectrum.

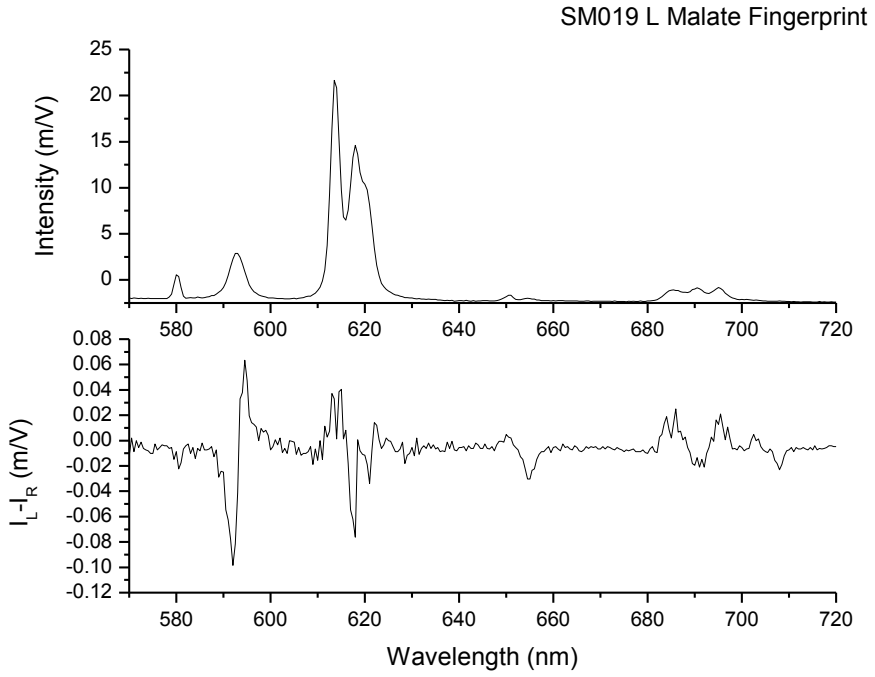

Figure 5.7: L malate Top: Total emission spectrum. Bottom: CPL spectrum

Spectra	g_{em} factor
D-malate	
CPL	-0.0006
L-malate	
CPL	-0.0006

Table 5.3 g_{em} factor for the MD transition of the total emission and CPL spectra for ΔJ = 2.

5.3.4 The Eu^{3+} 9N3 Complex in Presence of Citrate, Bicarbonate and Phthalate.

The observations previously made on the addition of D/L-lactate and D/L-malate to the Eu^{3+} 9N3 complex are repeated when a further set of racemic and achiral anions are added to the same complex. Varying degrees of intensity increases are observed which could be interpreted as electrostatic, but chirally unspecific interactions between the added anion and the Ln^{3+} complex. The evidence for this is the identical progression of the CPL for all these different anions.

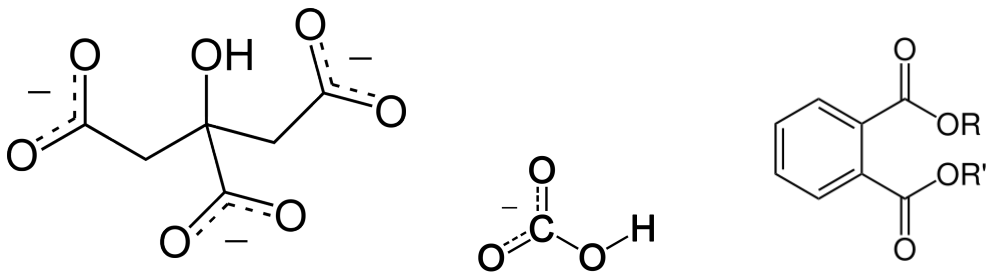

Figure 5.8 The structures of citrate, bicarbonate and phthalate

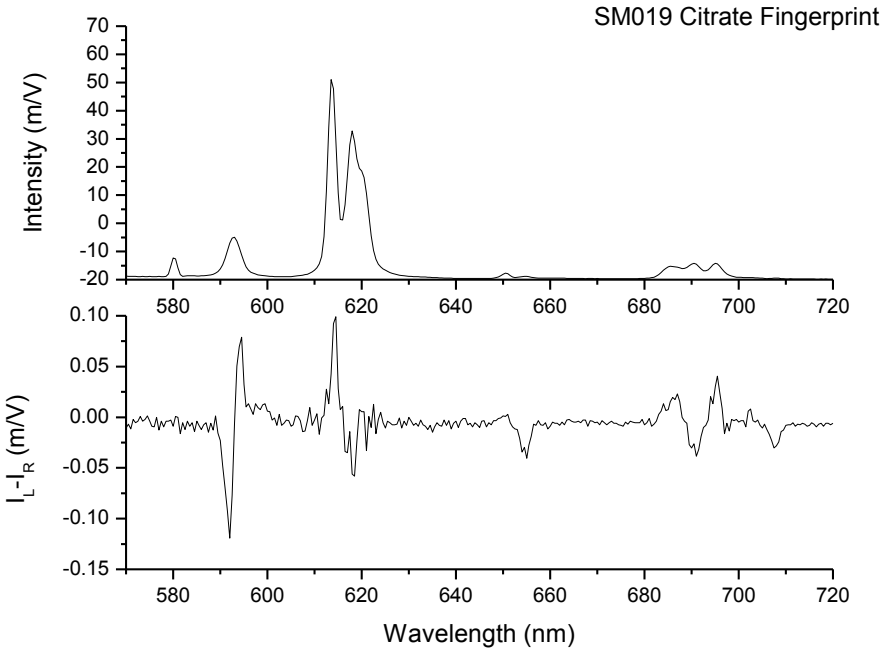

Figure 5.9: Citrate .Top: Total emission spectrum. Bottom: CPL spectrum.

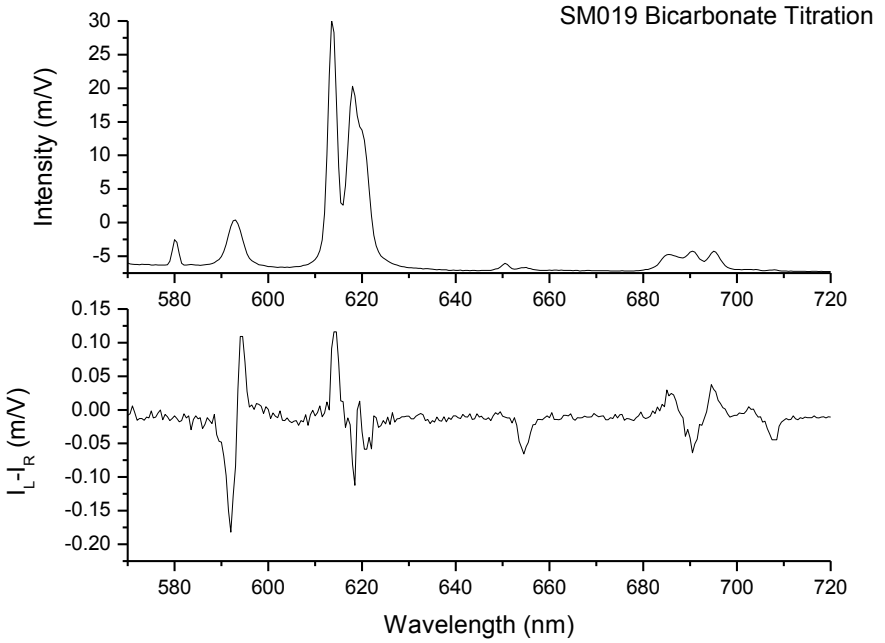

Figure 5.10: Bicarbonate titration. Top: Total emission spectrum. Bottom: CPL spectrum.

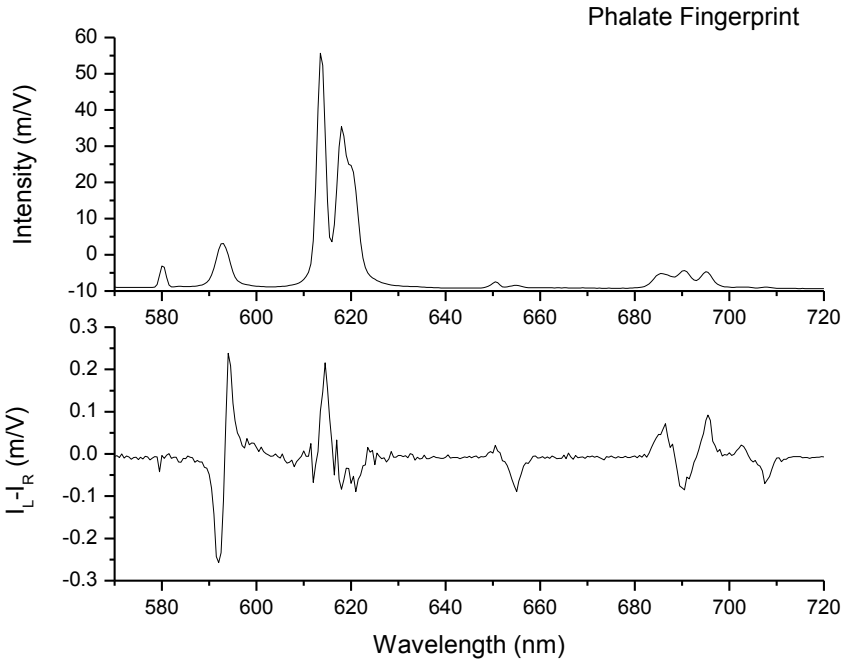

Figure 5.11: Phthalate. Top spectrum: Total emission. Bottom spectra: CPL spectrum

Spectra	g_{em} factor
Citrate	
CPL	0.0042
Bicarbonate	
CPL	0.0039
Phthalate	
CPL	0.0042

Table 5.3: g_{em} factor for the MD transition of the total emission and CPL spectra for ΔJ = 2

5.4 Conclusion

It can be concluded that switching on of CPL signal could be induced by addition of an anion to a Eu^{3+} complex. However, the studied complex, Eu^{3+} 9N3 do not interact

stereo-specifically to chiral anions. Hence, causing limitations for the use of the complex for these types of applications.

5.5 References

1. S. J. Butler and D. Parker, *Anion binding in water at lanthanide centres: from structure and selectivity to signalling and sensing*. Chem. Soc. Rev., 2013 **42,** 1652.
2. M. Iwamura, Y. R. Miyamoto and K. Nozaki, *Chiral sensing using an achiral europium (III) complex by induced circularly polarised luminescence.* Inorg. Chem. 2012, **51**, 4094-4098.
3. N. P. Barnes, *Lanthanide series lasers—near infrared. Handbook of Laser Technology and Applications* (Three- Volume Set).Dec 2003, 383 -410.
4. J. S. Stefaan, J. V. Greetje, K. Ashwini, H. Uwe, C. Marcel De, *Magnetoliposomes as magnetic resonance imaging contrast agents;* WIREs *Nanomed Nanobiotechnol*; 2011, **3**, 197-211.
5. S. Pandya, J. Yu and D. Parker, *Engineering emissive europium and terbium complexes for molecular imaging and sensing;* Dalton Trans., 2006, **23**, 2757-2766.

6. CPL MICROSCOPY DEVELOPMENT

6.1 Introduction.

Functionalised Ln^{3+} complex are versatile optical probes for sensing and imaging in biological systems such as assays and bio-active cells, as evidenced in many studies.[1,2,3] Their application in diverse methods of analysis such as luminescence spectroscopy is as a result of their unique magnetic and optical properties. Luminescence-based methods are particularly suited to the study of biochemical systems, because of the variety of possible applications and the fact this is a non-invasive technique. The compromise is the need to use an optical probe that will function as a signalling device. This can have the potential risk of compromising the integrity of the biological system. However, this can be avoided by using low concentrations of probe materials well below the so-called IC-50 value, which is the threshold for cell death. For functionalised Ln^{3+} complexes there is the added advantage that the polarisation of the emission can be monitored via the CPL signal. The potential advantages of this have been elaborated on previously with the prospect of studying stereo chemical interactions as the main benefit. In potential bio-imaging the advantages of CPL using functionalised Ln^{3+} complexes will be apparent with respect to avoidance of background auto fluorescence signals. This is due to the fact that the intra-cellular organic material that is responsible for auto fluorescence will very likely have a very small CPL. Typical g_{em} values for purely organic materials is in the 10^{-4} – 10^{-5} range.[4] With g_{em} values for chiral Ln^{3+} complexes potentially as high as 0.1 there will be a very good contrast between the background auto fluorescence and signal from the chiral Ln^{3+} complexes.

This sets the scene for a new concept, *microscopic sensing*, which is a novel methodology that can be used to probe the local environment in bio-active cells using optical PL microscopy based on CPL.

6.2 Towards Confocal CPL Microscopy.

6.2.1 The Layout of a Confocal CPL Microscope.

Figure 6.1 shows the layout for the bespoke CPL microscope. The first part of the development was to design and test an optical collection system that would result in the optimal collection of light.

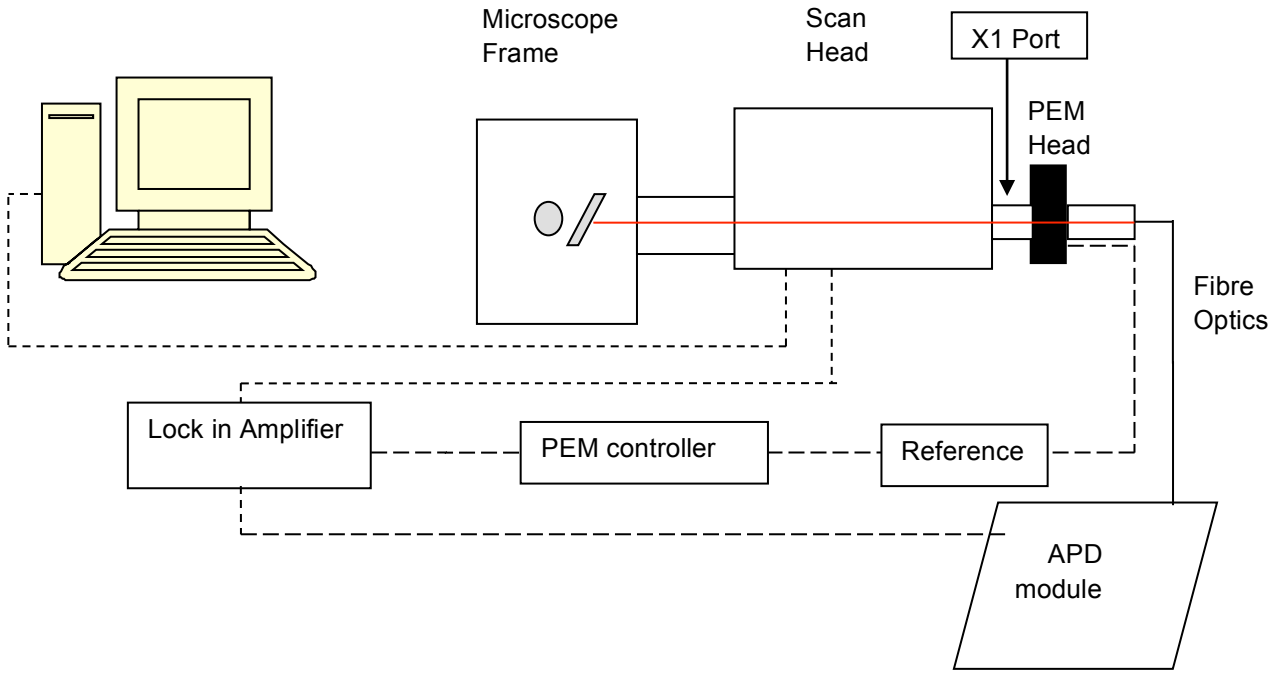

Figure 6.1: Schematic outline of the CPL microscope. Coloured line represents emission pathway and dashed lines represents electronic connections.

Tests on configurations were performed to determine a configuration and alignment of the collection adapter (fig 6.3) that would generate the maximum amount of transmitted light. 20 mm, 40 mm 63 mm lenses were used and tested in this pursuit. The external APD detection system connected to the X1port of the scan head and the image detected was referenced to the image obtained from the internal detection system. This is motivated by the optical layout of the X1 port which is shown in figure 6.2. The X1-port is a system fitted to the microscope that allows the observed PL signal obtained upon excitation from the microscope to be detected by an external detection system. An internal beam splitter selector allows for ratio detection between the internal and external detection systems, at 100 % or 95 % ratios relative to the external detector (fig 6.2). The difference in polarisation in PL signal (the CPL) shall be detected using a field modulation lock-in technique to obtain the CPL for the

electronic signal detection, see later section describing this approach. The beam towards the external detector diverges quite considerably (see Figure 6.2) and this calls for the need to introduce collection optics to focus the light on the fibre coupling which subsequently delivers the optical signal to the APD detection module.

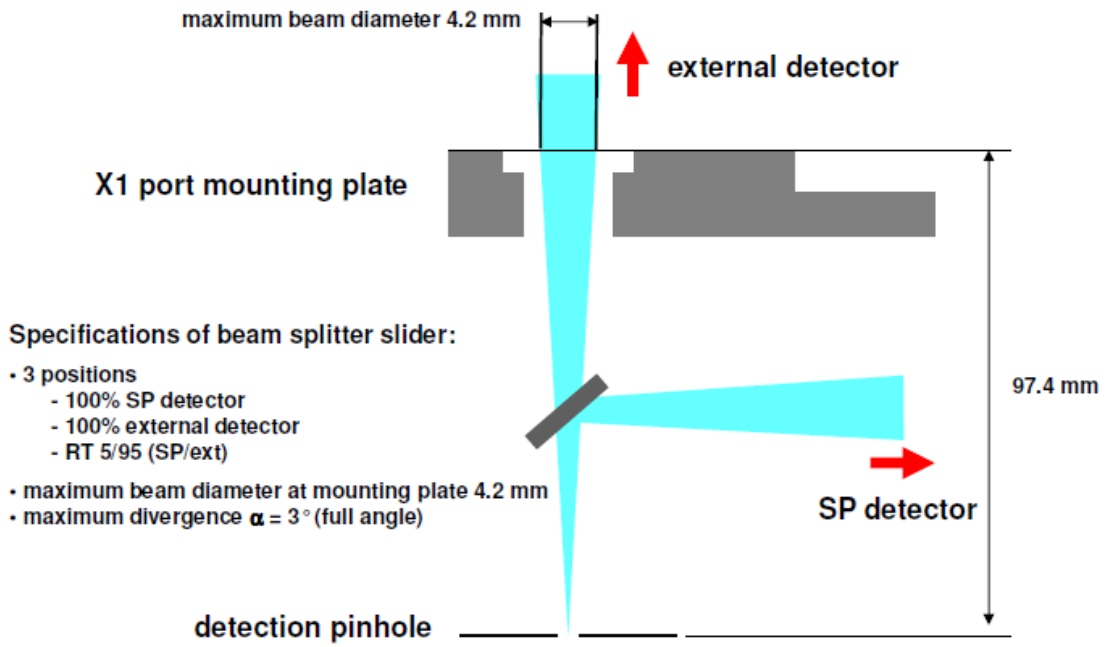

Figure 6.2 Optical layout of the X1 port. See text for details.

The configurations investigated were a combination of the different lenses and with and without the fibre coupling adapter unit shown in figure 6.3. In these comparisons, the PL of the sample materials was monitored in the same wavelength region for both the internal PMT systems and the external X1 port detection systems. For the X1 port detection system a suitable optical filter was used to select the relevant wavelength range. The CPL signal is detected in a similar fashion as described the steady state CPL spectrometer. Hence the CPL light propagates through the PEM and thereafter through a linear polariser, as shown in figure 3.1, and then further down the detection system.

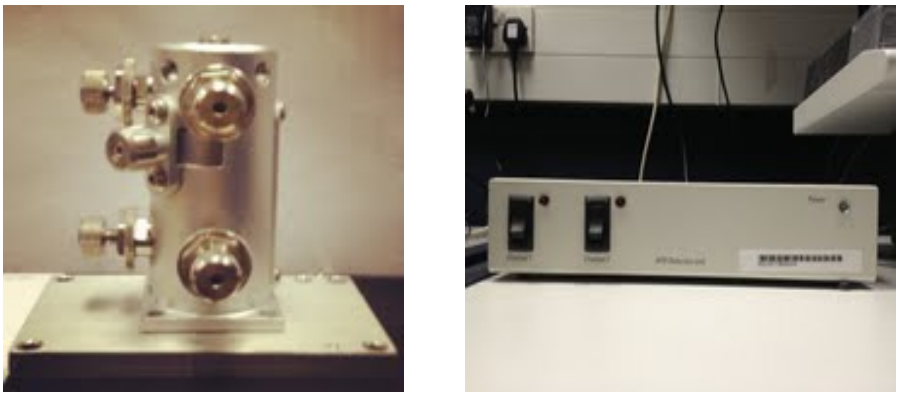

Figure 6.3. Left: Collection adapter unit. This adapter is mounted on the X1 port and connects the optical fibre to the APD unit where the optical signals are detected. Right: APD unit which converts the optical signals of the X1 port to electronic signal which are subsequently fed in the scanning system.

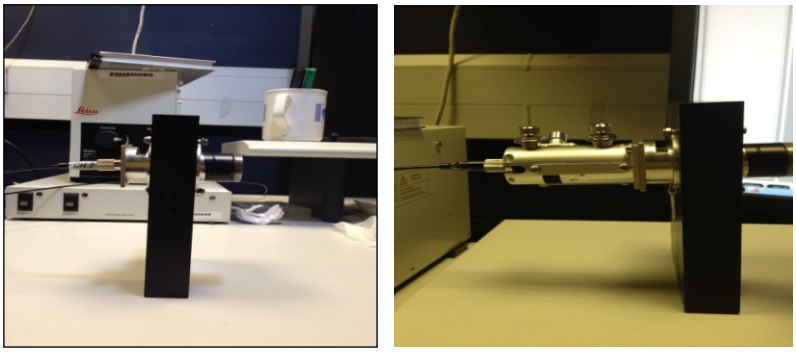

Figure 6.4. Left: Optical fibre directly connected to the PEM without adapter unit shown in fig **6.**3. Right: The PEM head with optical fibre attached to adapter unit.

Configuration 1

The test was tested with a 20 mm lens fixed into the adapter unit. The maximum power of laser light used was 18 % of total laser power available.

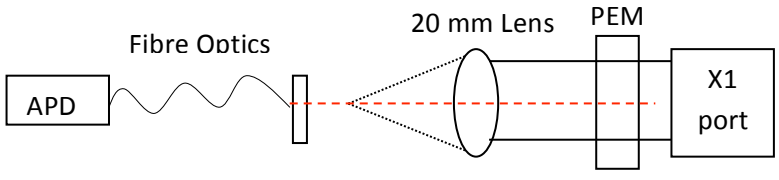

Figure 5.5. A 20 mm focal lens with adapter unit. Red dotted lines represent emission light.

Configuration 2

The second test was performed with a 63 mm lens fixed in the PEM with the adapter unit mounted to the PEM (figure 6.3). The maximum amount of laser power used for this configuration was 13 %.

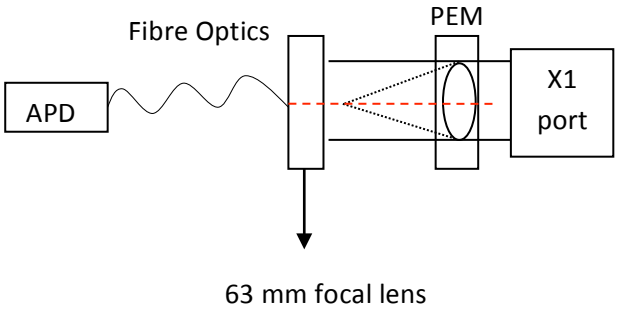

Figure 5.6. 63 mm focal lens with adapter unit. Red dotted lines represents emission light.

Configuration 3

The third test was performed with a combination with a 20 mm lens inserted to the PEM and a 40 mm lens inserted to the adapter unit.

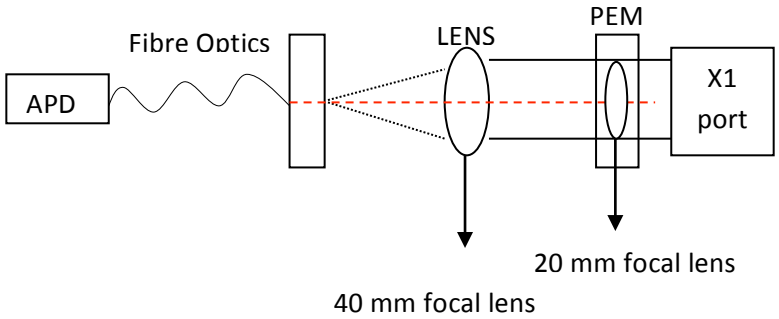

Figure 5.7. 40 mm focal lens and 20 mm lens with adapter unit. Red dotted lines represents emission light.

Configuration 4

The fourth test was performed with a 20 mm lens fixed into the PEM without the adapter unit.

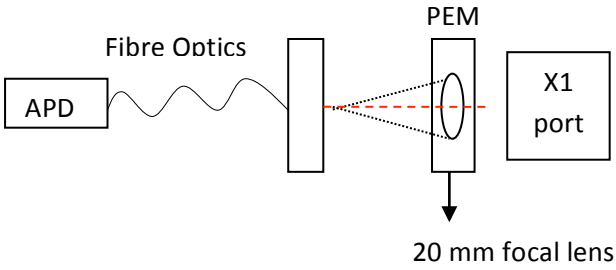

Figure 5.8: 20 mm lens without adapter unit. Red dotted lines represents laser light.

Configuration 5

The fifth test was performed with a 40 mm lens fixed in the PEM with the adapter.

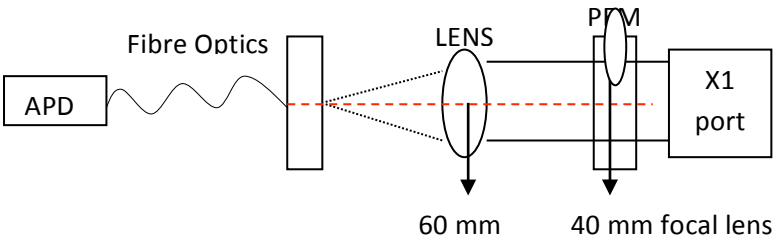

Figure 5.9. 40 mm and 60 mm lens with adapter unit.

The test was based on using the standard sample material (*Convallaria* Rhizome) provided by Leica Microsystems UK. Typical test conditions are listed in the table below.

Parameters	PMT	X1 PORT
Objective	20 x 0.7 oil	20 x 0.7 oil
Wavelength range	490-690 nm	490-690 nm
Resolution	512 x 512 PPI	512 x 512 PPI
Pinhole	36.01 µm	36.01 µm
Smart gain	646.7 V	13.3 %

Table 6.1 Microscope experimental parameters used in these test.

6.2.2 Results.

In other to determine the configuration that resulted in the optimal amount of light collected, the intensity ratio of the configuration was calculated. This was done by selecting the brightest spot on the image known as the region of interest (ROI). The mean of the ROI was calculated by the microscope software and the intensity ratio was calculated by dividing the mean value obtained for the X1 port image by the mean value of PMT image.

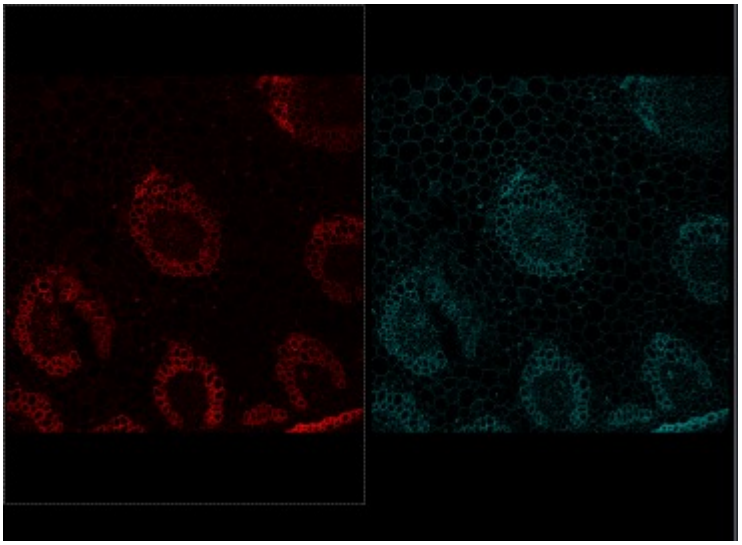

Figure 6.10. *Convallaria* Rhizome, t.s. Fast green Safranin. Right: PMT image. Left: Image obtained from X1port

The test material was a microscope slide with fixed cells (*Convallaria* Rhizome), stained with a variety of different optical probes that allows for wide choice of excitation wavelengths leading to broad range of PL emission wavelengths (provided by Leica Microsystems UK). For these experiments the same excitation wavelength was used though out the tests,

Configuration	Mean value (PMT)			Mean value (X1 port)			Intensity ratio (IR)			Average IR
	ROI 1	ROI 2	ROI 3	ROI 1	ROI 2	ROI 3	ROI 1	ROI 2	ROI 3	
1	10.99	8.77	8.27	34.42	22.15	26.30	3.13	2.52	3.18	2.94
2	10.18	8.79	8.27	22.72	17.63	18.41	2.23	2.00	2.22	2.15
3	8.64	7.94	6.87	1.02	0.88	1.01	0.11	0.11	0.14	0.12
4	8.96	8.63	7.63	0.81	0.69	0.64	0.09	0.08	0.08	0.08
5	8.90	7.47	6.78	3.78	3.56	2.50	0.42	0.47	0.36	0.42

Table 6.2 The intensity ratios of three different spots of the same image in each configuration was calculated

6.2.3 Conclusion.

Based on the data obtained above, the brightest region was obtained from configuration 1. Hence future work shall likely be done using this configuration. Configuration 1 was done with 18 % of the laser power which is in fact very low excitation intensity. This indicates that there is still room for increasing the intensity.

The experiments also show clearly that there is no distortion of the images due the additional optical elements.

6.2.4 Electronic Design of the Signal Acquisition System.

Future work will focused on pursuing the electronic detection of the CPL signal obtained from the APD. The block diagram of the signal pathway is shown in figure 5.11. As can be seen the signals going in to the LIA has TTL character. However, the output of the LIA is of NIM character. Hence it will be necessary to convert from NIM to TTL as this the required format that must be fed into the microscope scanning system. This shall be done by finding or designing a suitable converter, which will be designed by the electronic workshop engineers at Durham Universty.

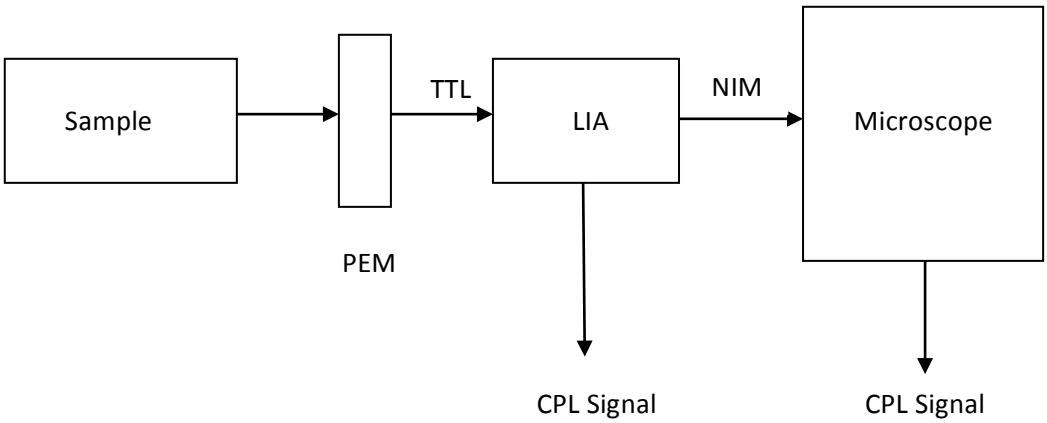

Fig 6.11 1st step: emitted light from the sample goes to the PEM then to LIA (CPL signal). 2nd step is to feed the signal into the microscope to see second CPL signal. NIM has to be converted to TTL.

The next immediate step is to try to detect a CPL sensitive signal directly from the LIA without feeding this signal into the microscope scanning system. A suitable chiral emitter or an artificial CPL signal using a quarter wave plate shall be used for this purpose. The aim of this is to confirm the workings of the optical and part of the electronic detection system and to get an idea of the signal intensities that will be available.

6.3 Estimated CPL Signal Intensities.

What kind of signal intensities can be expected in CPL microscopy? This aspect is necessary to consider if this is a possible new methodology that can be used successfully in bio imaging of biological systems using functionalised Ln^{3+} complexes. The success to this will depend on the magnitude of the g_{em} factor, the intensity (PLQY) of the Ln^{3+} complex used and the background noise due the microscope detection system.

This shall be estimated based on a microscope image obtained for CHO cells doped with a functionalised Eu^{3+} complex. This image is shown in figure 6.12.

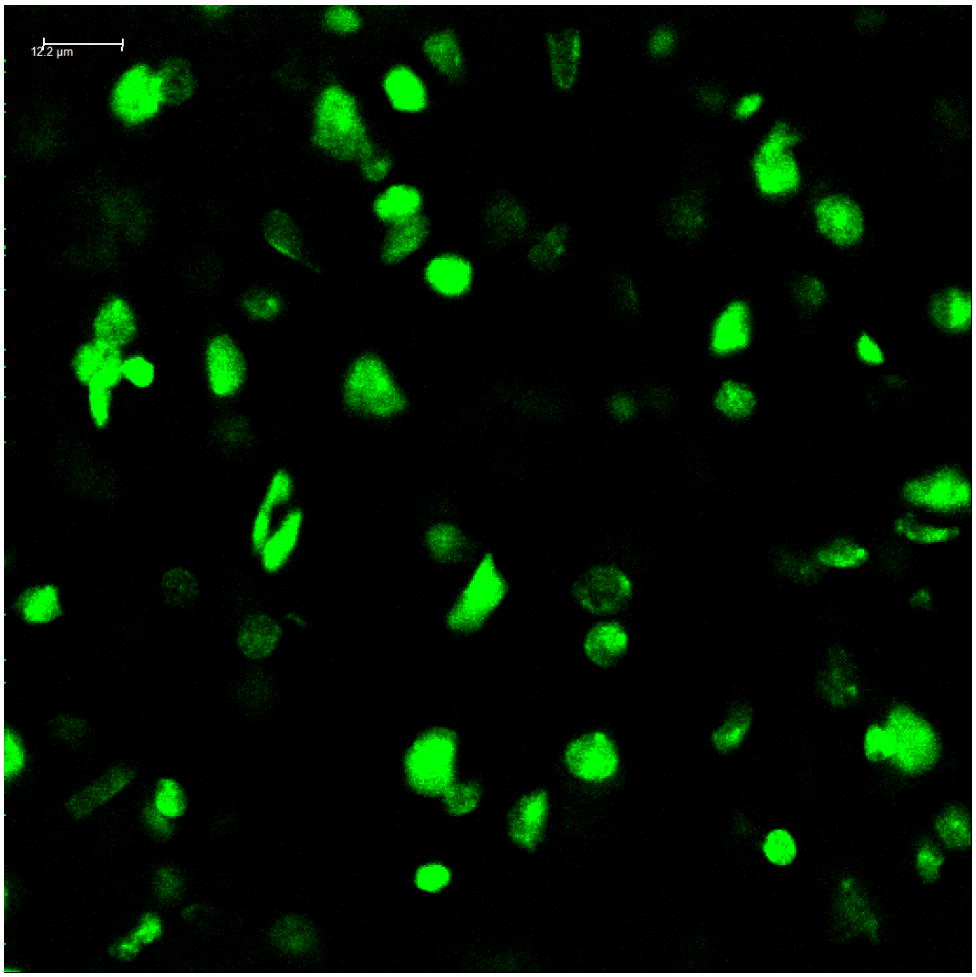

Figure 6.12 Image from life cell imagimng of CHO cells using an Eu^{3+} complex. This image was provided by Dr L-O Pålsson of Durham Universty.

From a ROI analysis of the image above we obtain the following intensity parameters; detection background noise ~ 5-10 counts (dark areas in the image), signal from stained cell(s) ~ 2500 counts.

The emission dissymmetry factor is given by the equation below (previously defined in chapter 2 (equation 2.10)

$$g_{em}(\lambda) = \frac{2\left[I_L(\lambda) - I_R(\lambda)\right]}{I_L(\lambda) + I_R(\lambda)} \qquad \text{eqn (6.1)}$$

, the intensity differences of $\left[I_L(\lambda) - I_R(\lambda)\right]$ can be estimated. Suppose a generic chiral Ln^{3+} complex display similar PLQY and has an emission dissymmetry factor g_{em} = 0.1.

Inserting these values into equation 6.1 with $\left[I_L(\lambda)+I_R(\lambda)\right]=2500$ will result in a difference signal that is $\left[I_L(\lambda)-I_R(\lambda)\right]=125$. This is more than a factor ~10 above the detection system noise level. Hence, it realistic to conclude that a non-zero CPL signal should be observed in a bio-imaging experiment on a live cell using chiral emissive functionalised Ln^{3+} complexes.

6.4 References.

1. G. Muller, *Luminescent chiral lanthanide(III) complexes as potential molecular probes,* Dalton Trans., 2009, 44, 9692-9707.
2. J. G. Bünzli and C. Piguet, *Taking advantage of luminescent lanthanide ions*, Chem. Soc. Rev, 2005, 34, 1048-1077.
3. R. A. Poole, G. Bobba, M. J. Cann, J. Frias, D. Parker and R. D. Peacock, *Synthesis and characterisation of highly emissive and kinetically stable lanthanide complexes suitable for usage 'in cellulo*', Org. Biomol. Chem., 2005, 3, 1013-1024.
4. R. Carr, N. H. Evans and D. Parker, *Lanthanide complexes as chiral probes exploiting circularly polarized luminescence*, Chem. Soc. Rev., 2012, 41, 7673–7686.

APPENDICES

LIST OF SEMINARS ATTENDED

Seminars:

01/05/12	Prof. David Parker	Lanthanide coordination chemistry; probe, excite, measure, relax
13/06/12	Gemma Freeman	Understanding the surprising emission properties of a new series of Pt(II) complexes
13/06/12	Rachael Harder	Fluorescence of Carboranes
10/01/13	Professor Rob Short	Surfaces for Regenerative Medicine